Available online at www.sciencedirect.com
ScienceDirect
Icarus 195 (2008) 317–339
ICARUS
www.elsevier.com/locate/icarus

A meteoroid stream survey using the Canadian Meteor Orbit Radar I. Methodology and radiant catalogue

P. Brown *, R.J. Weryk, D.K. Wong, J. Jones

Department of Physics and Astronomy, University of Western Ontario, London, Ontario N6A 3K7, Canada

Received 26 September 2007; revised 28 November 2007

Available online 23 December 2007

Abstract

Using a meteor orbit radar, a total of more than 2.5 million meteoroids with masses $\sim 10^{-7}$ kg have had orbits measured in the interval 2002–2006. From these data, a total of 45 meteoroid streams have been identified using a wavelet transform approach to isolate enhancements in radiant density in geocentric coordinates. Of the recorded streams, 12 are previously unreported or unrecognized. The survey finds >90% of all meteoroids at this size range are part of the sporadic meteoroid background. A large fraction of the radar detected streams have $q < 0.15$ AU suggestive of a strong contribution from sungrazing comets to the meteoroid stream population currently intersecting the Earth. We find a remarkably long period of activity for the Taurid shower (almost half the year as a clearly definable radiant) and several streams notable for a high proportion of small meteoroids only, among these a strong new shower in January at the time of the Quadrantids (January Leonids). A new shower (Epsilon Perseids) has also been identified with orbital elements almost identical to Comet 96P/Machholz.

Keywords: Meteors; Radar observations; Orbit determination; Interplanetary dust

1. Introduction

Understanding the linkage between meteoroids and their parent bodies is a major goal in meteor astronomy. The evolution of meteoroids, their physical properties and their mass distribution all contribute substantially to our knowledge of comets (and potentially asteroids), providing insights into parent body mass loss mechanisms (Jenniskens, 1994), periods of past activity (Wiegert and Brown, 2004), chemistry (Borovicka et al., 2005) and previous orbital history (Vaubaillon and Jenniskens, 2007). Direct measurements of short-period comet dust trails (Reach et al., 2007), for example, have established quantitative estimates for solid particle mass loss and support the notion that mm-cm-sized debris is the principle mode of short-period cometary mass loss. This finding has played a key role in modifying the standard paradigm of comets as dirty snowballs into (at least some) comets being more akin to "frozen mudballs" (Sykes and Walker, 1992).

Of all the techniques used to measure the meteoroid population in cometary dust trails, direct detection in Earth's atmosphere is the most sensitive. Meteors observed ablating in the Earth's atmosphere allow individual meteoroid orbits to be measured with high precision (Betlem et al., 1997) and fluxes/spectroscopically determined chemistry of individual meteoroids may be related back to specific parent bodies. Performing the latter task requires knowledge of a particular meteoroid's parent, which in turn requires establishing membership in a meteor shower.

The physical characteristics of meteor showers has been a major area of study in meteor science since individual meteor showers were first recognized in the mid-18th century (Burke, 1986). A proliferation in the population of potential meteor showers in the early 20th century is exemplified by the numerous shower catalogues published in this area (cf. Hoffmeister, 1948; Denning, 1899).

As the decay products of comets and possibly asteroids, meteor showers offer a unique window into the origin and evolutionary processes of small Solar System bodies which have orbits close to the Earth. The age of meteor showers constrain the residence time for specific comets in the inner Solar System,

* Corresponding author. Fax: +1 519 661 4085.
E-mail address: pbrown@uwo.ca (P. Brown).

0019-1035/$ – see front matter
doi:10.1016/j.icarus.2007.12.002

the radiant spread within a young shower may offer insight into the ejection speeds for meteoroid-sized particles at the comet, the ablation behavior of specific meteor showers reveal differences in parent body strengths/compositions and evolution while the mass estimates of showers provide lower limits to parent body masses (cf. Jenniskens, 2006). In some cases, the very existence of a meteor shower may be the first clue that a potentially hazardous asteroid or comet exists, with the orbit of the shower providing the telling evidence needed to make a link, as was the case for the Geminids and Phaethon (Whipple, 1983) and 2003 EH1 and the Quadrantid meteor shower (Jenniskens, 2004). Linking meteoroid streams to parent asteroids provides a direct means of estimating the proportion of extinct cometary nuclei amongst the near-Earth asteroids. Making these linkages often requires extensive backward orbital integrations which in turn requires precise knowledge of a streams orbit.

Given the importance of meteor showers to studies of small Solar System bodies, establishing clearly the existence of both major and minor showers and characterizing their essential parameters (radiant locations, drifts, velocities, orbits) would therefore seem to be a critical first step. Numerous studies have attempted just this exercise in the past, with varying degrees of success. A common problem with many past surveys (which are briefly summarized in the next section) are lack of statistics and temporal coverage. While the major showers which are universally recognized show up in most surveys, the characteristics of these showers often are uncertain, their linkage to other showers unclear and the case for the existence of minor showers is often not compelling. In many surveys, correspondence between as few as two orbits is taken as evidence for a new shower association, despite the fact that observational errors may make the majority of such associations purely chance.

Here we describe a seven year survey of meteor showers as detected with the Canadian Meteor Orbit Radar (CMOR). In developing our methodology, our intent is to establish a listing of meaningful major and minor meteor showers which are unambiguously detected in multiple years, with multiple radar frequencies and using two distinct detection methodologies derived from a large orbital database. Separate papers will present the flux and mass distribution for the showers found in this initial survey paper.

In total more than 2 million orbits are examined together with more than 18 million individual meteor echoes observed from one radar station over the period 2000–2006. We recognize that other minor streams exist in this dataset, but wish to be conservative in our detection criteria such that this initial list consists of only showers for which there is high confidence in their existence. As additional data are collected, we expect additional showers to be added to this provisional CMOR list.

In Section 2 we review the major past surveys of meteor showers and describe criteria for detection used in previous works. Section 3 briefly outlines the operation of CMOR and Section 4 details our analysis techniques. Section 5 summarizes the results of applying these analysis routines to our dataset while Section 6 compares our results to past studies. In Section 7 we summarize our main findings and present conclusions.

2. Previous meteor shower surveys

The earliest meteor shower catalogues were entirely based on visual observations (cf. Denning, 1899; Hoffmeister, 1948; McIntosh, 1935). These early compilations relied on plots of meteor paths as seen by one observer and an apparent intersection of several trails in a radiant "area." This procedure produced thousands of radiants; today it is recognized that most were spurious (cf. Jenniskens, 2006). With the exception of the major annual showers and rare outbursts and/or storms (where hourly rates were high relative to the average sporadic background), few other showers were known prior to the middle of the 20th century with any reliability.

The major revolution in meteor shower determination came about through application of new observational techniques. The photographic surveys (most notably that from the Harvard Super Schmidt Program; Whipple, 1951) and radar measurements (cf. Lovell, 1954) allowed systematic instrumental records to be gathered and individual meteor trajectories/orbits determined with a precision far beyond that possible with visual observations. The majority of earlier visual showers were refuted through examination of this early data and new lists of showers compiled based on these instrumental records (cf. Cook, 1973). The main surveys and datasets producing large numbers of radiants and orbits for meteors, which have formed the basis for almost all subsequent meteor shower searches, are summarized in Table 1.

Given these higher precision data, the next step is to decide what, precisely constitutes a meteor shower. The quantitative definitions used previously have usually relied on similarity in orbital parameters as a means to establish membership in a stream and mean shower orbital elements to establish association with a putative parent body.

The earliest quantitative measures of orbital similarity for meteoroid orbits was proposed by Southworth and Hawkins (1963), now termed D_{SH}. They chose to use all orbital elements defining the shape and orientation of an orbit in making shower associations (rather than radiants, geocentric velocities and time of occurrence alone) because their dataset of interest had only 359 orbits and the data were of high precision. This criteria has been widely employed (cf. Lindblad, 1971; Jopek and Froeschle, 1997, among many others) for the purpose of stream identification. Drummond (1981) introduced a modified version of the D_{SH} (D_D) using chords rather than angles and normalization of eccentricity and perihelion terms in D_{SH} as an attempt to remove the heavy bias introduced into D_{SH} for streams with large perihelion distances or eccentricities.

The essence of these (and many subsequent) orbital association techniques is to measure distances in orbital element phase space and choose a region around a given test point and define that region as "significantly" associated with the test point. These approaches depend on choosing the correct size for the region of significance. Unfortunately, the errors in orbital elements are not uniform for all measured meteors—higher entry velocity meteoroids typically have larger spreads in all elements due to higher absolute errors in determined velocity. The cut-off values for regions of significance need to be scaled with im-

Table 1
Major surveys measuring meteoroid orbits, based partially on the compilation of Baggaley (1995) and Lindblad et al. (2003)

Type	Location	Years	N_{orb}	LM	References
Photo	Massachusetts, USA New Mexico, USA	1936–1952	171	∼0	Whipple (1954)
Photo	Dushanbe, USSR	1940–1983	639	∼ +1	Katasev (1964); Babadzhanov and Kramer (1967); Lindblad et al. (2003)
Photo	New Mexico, USA	1952–1959	1332	+2	Jacchia and Whipple (1961); Hawkins and Southworth (1961); McCrosky and Posen (1961)
Photo	Ondrejov, Czechoslovakia	1955–1959	109	+3	Ceplecha et al. (1964); Ceplecha (1957)
Photo	Central Europe (EN)	1955–1990	189	−6	Oberst et al. (1998)
Photo	Kiev, USSR	1957–1981	206	∼ +1	Lindblad et al. (2003)
Photo	Odessa, USSR	1957–1983	459	∼ +1	Babadzhanov and Kramer (1967); Lindblad et al. (2003)
Radar	Jodrell Bank, UK	1954–1955	2509	+7	Davies and Gill (1960)
Radar	Adelaide, Australia	1960–1961	2092	+6	Nilsson (1964)
Radar	Kharkov, Ukraine	1960–1965	12500	+7	Lebedinets (1968)
Radar	Illinois, USA	1961–1965	19327	+10	Verniani (1973); Sekanina (1973)
Photo	Western USA (PN)	1963–1975	334	−3	McCrosky et al. (1978)
Photo	Japan (TMN)	1964–1989	339	∼ +2	Lindblad et al. (2003)
Radar	Obninsk, USSR	1967–1968	9358	+7.5	Lebedinets et al. (1981, 1982)
Radar	Kazan, USSR	1968	3200	+8	Andrianov et al. (1968, 1970)
Radar	Adelaide, Australia	1968–1969	1667	+8	Gartrell and Elford (1975)
Radar	Illinois, USA	1968–1969	19818	+10	Verniani (1973); Sekanina (1976)
Radar	Mogadisho, Somalia	1968–1970	5328	+8	Fedynski (1975, 1977)
Photo	Western Canada (MORP)	1971–1985	365	−5	Halliday et al. (1996); Halliday (1988); Campbell-Brown and Hildebrand (2004)
Photo	Netherlands (DMS)	1972–2001	1344	∼0	Lindblad (1987); Lindblad (1991)
Photo	New Mexico, USA	1974–1977	25	∼0	Tedesco and Harvey (1976)
Radar	Kharkov, USSR	1975	5317	+12	Kashcheev and Tkachuk (1980)
TV	London, Canada	1981–1982	454	+8.5	Sarma and Jones (1985)
TV	Netherlands (DMS)	1991–2000	1112	+6	Lindblad (1987); Lindblad (1991)
Radar	Christchurch, New Zealand	1990–1994	3×10^5	+13	Baggaley et al. (1994)
Radar	Christchurch, New Zealand	1995–1999	5×10^5	+14	Galligan and Baggaley (2005)
TV	Japan (NMS)	1998–1999	263	+7	Ueda et al. (2001)
TV	Ondrejov, Czech Republic	1998–2001	496	+5	Koten et al. (2004)
Radar	London, Canada	2002–2007	2×10^6	+8	Present study

Type indicates the method of data collection. The LM column refers to the approximate equivalent meteor limiting magnitude of the survey.

pacting speed. For this reason, these approaches are prone to error and (particularly) poorly suited to datasets having large spreads in speeds, such as those measured by radar (as opposed to more precisely determined photographic data) (see Jopek, 1993; Galligan, 2000, for a review).

Valsecchi et al. (1999) introduced a different orbital similarity criterion having the advantage that it is based on the directly measured geocentric quantities of a meteoroid orbit; the geocentric velocity and radiant as well as the time of occurrence of a meteor. Their criteria allows tests of orbital similarity using four measured quantities for a meteoroid orbit, two of which are invariant over the short timescales typical of meteoroid stream coherence. Their application of this new similarity function shows it to be both complementary and superior in many ways to the previously mentioned D_{SH} and D_D functions (cf. Jopek et al., 1999) suggesting use of these geocentric quantities is a natural means to identify clustering in meteor data.

Galligan and Baggaley (2002a) have examined the orbital data gathered over a five year period by the Advanced Meteor Orbit Radar (AMOR) and applied various cluster search techniques to try to identify streams in their data. They applied a wavelet transform (described later) to the radiant locations of individually measured orbits with further partitioning of the radiant data by time of occurrence and velocity to strengthen localized enhancements potentially due to showers. They were able to isolate six streams with certainty using this approach; their search technique is largely equivalent to that used by Valsecchi et al. (1999).

In what follows we have used an equivalent series of quantities to those proposed by Valsecchi et al. (1999) to examine clustering in our suite of radar orbits. Our approach has been largely inspired by the work of Galligan and Baggaley (2002a) and we follow much of their methodology with appropriate modifications particular to our dataset. AMOR is sensitive to meteoroids ∼100 times smaller in mass than CMOR and hence tends to be most efficient at detecting sporadic meteoroids (which have a steeper mass distribution than showers, which are richer in larger meteoroids). CMOR is thus expected to have a larger fraction of detected meteoroids in identifiable streams.

3. CMOR: Overview of operations, data collection and analysis

The Canadian Meteor Orbit Radar (CMOR) consists of three separate interferometric radars, synchronized in transmission and reflection operating from a single site. Details of the system can be found in Jones et al. (2005) and Webster et al. (2004); here we provide a brief overview only.

The three systems operate at 17.45, 29.85 and 38.15 MHz. The receive and transmit hardware are commercially available SKiYMET systems (Hocking et al., 2001). The "orbit" com-

ponent of the system applies only to the 29.85 MHz system which has two outlying remote stations (6.2 and 8.1 km respectively from the main site) providing reflections from portions of the trail not directly accessible from the specular reflections to the main site. For these echoes, the interferometry from the main site, when combined with the time delay from each remote site is sufficient information to permit measurement of velocity vectors for individual meteors. Traditionally, multi-station radars have been used to determine meteoroid orbits using a method first proposed by Kaiser. This technique (time-of-flight) has been widely used for orbit determination by other radar surveys (cf. Sekanina, 1973; Nilsson, 1964). The method relies on a combination of meteoroid speeds derived from the measurement of the Fresnel oscillations in the echo amplitude and the time delays measured between a main central station and two non-collinear outlying stations. Because only a small fraction of the detected echoes produce measurable Fresnel oscillations, there is some question whether the orbital distributions so obtained are representative of the whole set. The design of both the AMOR and CMOR radars takes a different approach: in addition to the time delays, interferometry is used to determine the directions of the echoes which are known to be orthogonal to the meteoroid trajectories. By doing this, the dependence on the Fresnel method of determining meteoroid speeds is avoided and orbits can be determined for all the echoes detected.

The principle difference between earlier surveys and the measurements made by CMOR is that we do not require Fresnel oscillations in amplitude to measure the time offsets; rather we make use of a common reference point found on the rising edge of the filtered echo (which removes high frequency fluctuations) at each site where the inflection point has a minimum in the 2nd derivative of the amplitude vs time profile.

Velocities are also measured for ∼5% of all echoes using the hybrid-Fresnel oscillation method of Hocking (2000) from single station data. These echoes, however, do not have complete individual trajectory information from this velocity information alone.

The configuration details common to all three systems are given in Table 2. Each system has seven antenna and seven separate receivers. For the 17 and 38 MHz systems all seven receivers are used for reception (to boost signal to noise levels) but only five are used for determination of measured echo direction using interferometry. The 29 MHz system uses the two extra receivers to record signals from the two outlying stations.

Table 2
CMOR hardware and operating characteristics

Quantity (units)	17.45 MHz	29.85 MHz	38.15 MHz
Location (latitude, longitude) (degrees)		43.264° N, 80.772° W	
Pulse repetition frequency (Hz)		532	
Range sampling interval (km)		15–252	
Range resolution (km)		3.0	
Peak transmitter power (kW)		6.0	
Transmitter half bandwidth to 3 dB points (kHz)		30.0	
Receiver half bandwidth to 3 dB points (kHz)		25.0	
Transmit pulse length (μs)		75.0	
Receiver noise level (dBm)	−98	−109	−113
Receiver absolute (noise limited) equivalent meteor limiting magnitude	+7.4	+8.8	+9.3

The transmit and receive antenna have broad (nearly all-sky) gain patterns. The transmit antenna is a vertically directed, horizontally-polarized 3 element Yagi with $G = 7.6$ dB$_i$ (relative to an isotropic radiator) and a beam width to the 3 dB points of 30°. The receive antennae are all two element, vertically directed horizontally-polarized Yagis with $G = 6.5$ dB$_i$ and beam-widths of 45° to the 3 dB points. Directions to each echo are measured using the relative phase difference between the antennae within each of the 5-element interferometer arrays (cf. Jones et al., 1998, for more details of the interferometry technique). The interferometric error is less than 0.5° for echoes with elevations above 30° found through simulation for echoes with SNRs above 15 dB. Due to the degradation in interferometric accuracy at low elevations, no echoes are processed if their nominal elevation is below 20°.

The basic echo detection and analysis algorithms used for the SKiYMET system are described in detail in Hocking et al. (2001). Once an echo is detected at the main site various characteristics are measured including time of occurrence, interferometric location, range, height, lifetime and maximum amplitude. The occurrence time is recorded to a precision of 1 ms and locked to a GPS clock, though the systematic offset of the system is such that accuracies can be as poor as ∼1 s in extreme cases (though all systems have the same offset when present) due to delays caused by hardware interrupts.

For the 29.85 MHz orbital system, each remote link signal is saved on the two extra receiver channels at the main site after being transmitted over a UHF link. Approximately 1/4 of all echoes detected at the main site on 29.85 MHz have the correct geometry and sufficient signal strength as seen from both remote sites to allow time delay measurements and orbit calculation.

All receivers are cosmic noise limited, with minimal detectable signal strengths as given in Table 2. The variation in noise levels is controlled principally by galactic cosmic noise at our HF/VHF frequencies and produces a diurnal noise variation of 2 dB for 29 and 38 MHz. The 17.45 MHz system suffers from heavy terrestrial interference during the day limiting useful echo detections to night-time hours only.

Single-station data collection with CMOR began in 1999 with orbit capability added in early 2002. In recent years the uptime duty cycle of the radar has exceeded 90%, with the orbit measurement duty cycle only slightly lower. The daily number of detected echoes from each of the three systems is shown in Fig. 1. During the entire period of the survey, each of 17.45, 29.85 and 38.15 MHz recorded 26.3, 18.3 and 11.0 million meteor echoes respectively.

For the 29.85 MHz orbital system, the absolute minimal detectable signal strength corresponds to meteors with radio magnitudes near +9 (cf. Verniani, 1973, for the definition of radar meteor magnitude). However, effective counting statistics for 29.85 MHz are complete only to +8 due to the roll-off in sensitivity as the absolute detection threshold is reached—this is the

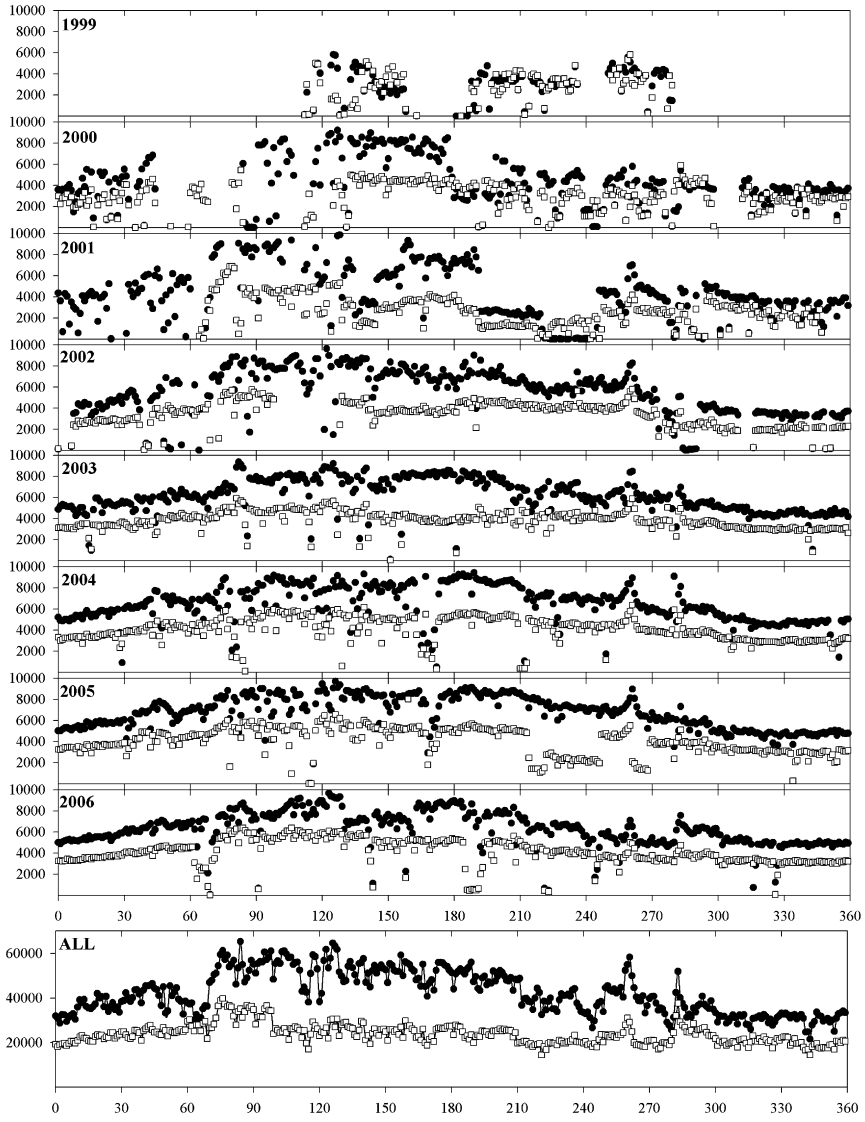

Fig. 1. The number of detected echoes on 29 MHz (solid circles) and at 38 MHz (open squares) as a function of solar longitude from 1999–2006. The irregular distribution in 1999–2001 is due to periodic downtime experienced by the radars; all systems were significantly more stable from 2002 onwards. The final graph (bottom) represents the total echoes per degree solar longitude bin detected from 1999–2006.

effective detection limit for the radar and corresponds to meteoroids of $\sim 10^{-7}$ kg mass for an average velocity of 30 km/s. Fig. 2 shows the number of orbits measured each day since the orbital system began operation. The total number of unique orbits measured to mid-2007 is just over 2.5 million.

The distribution of magnitudes for each echo with a measured orbit is shown in Fig. 3. Here the velocity measured using the time-of-flight technique is combined with the received echo power and the gain in the direction of the echo to estimate mass using the mass–magnitude–velocity relation of Verniani (1973). The value is a lower limit to the actual mass as we implicitly assume the scattering occurs at the point of maximum ionization. Note that the distribution has not been corrected for biases and merely represents the magnitude distribution of meteors having orbits measured with our radar system—it should not be used to quantitatively compute mass distribution indices (for example) in raw form.

The receivers have automatic phase calibrations performed every $\frac{1}{2}$ hour during radar operation. Typical daily variations in the receiver phases are measured to be of order a few tenths of a degree. The phase difference introduced through cabling is a larger source of uncertainty. End-to-end phase calibrations are made a few times per year and typically show differences of order 2°–3° over the course of several months. Transmitter power on 29 and 38 MHz is measured every 10 min using two Bird 4391A Wattmeters with precisions of 5%. Power variations are less than the measurement precision and generally exceed this threshold only when significant impedance mismatches occur between the cabling and transmit antenna, such as during ice storms. Considering all sources of error, we estimate our interferometric measurements to be accurate $<0.5°$ for most echoes at elevations above 30°.

Our main source of error in velocity and radiant measurements are due to uncertainties in the measured time delays between the main and remote sites (cf. Jones et al., 2005, for

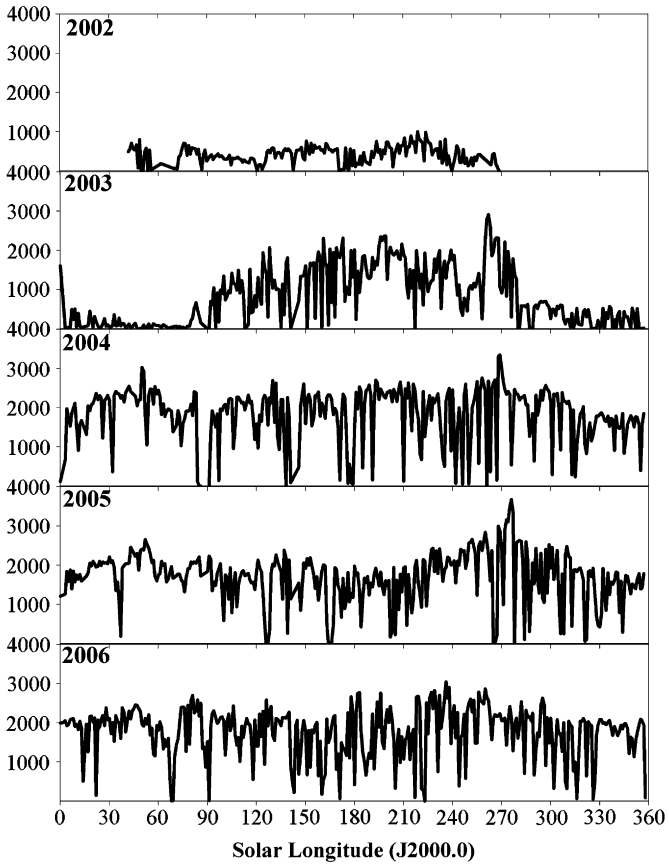

Fig. 2. The number of orbits measured per degree of solar longitude from 2002–2006.

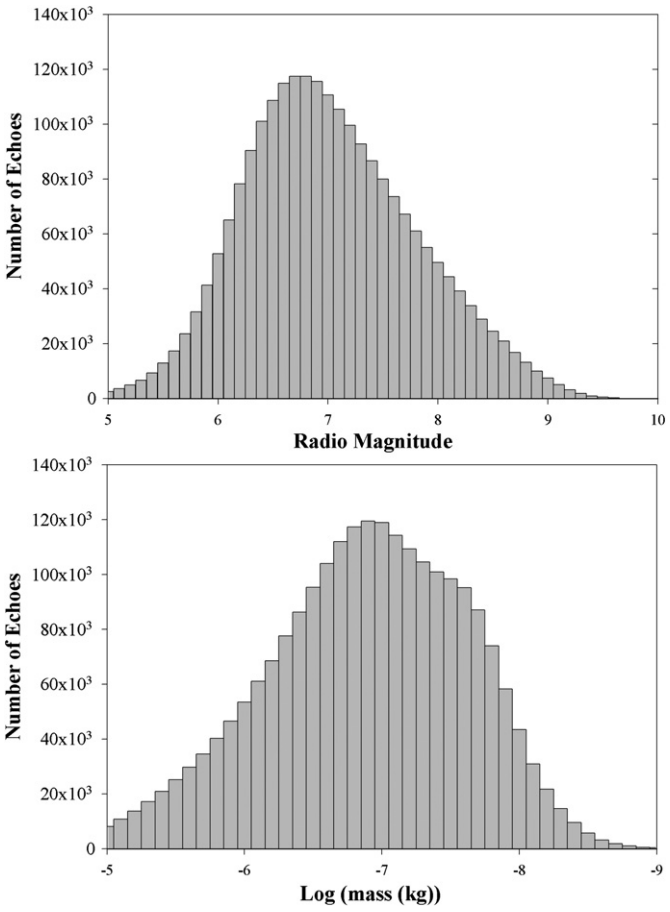

Fig. 3. The magnitude distribution (top) and mass distribution (bottom) for all radar echoes where orbits have been measured. The electron line density–mass–magnitude–velocity relation from Verniani (1973) has been used. Note that these values are upper limits as we assume scattering occurs at the point of maximum electron line density.

a more complete discussion of this point). The uncertainty in this value depends on the character and shape of each echo and may vary considerably—we cannot specify this for each echo. The impact of a given time delay measurement error on radiant and velocity determination also depends on the echo geometry. An error of one pulse in the time delays corresponds very approximately to an error in radiant direction of 2° and a velocity error of 3% at 40 km/s. In practice, we find our radiant spread and velocity errors are larger by about a factor of two than these values. This best estimate for our mean error is found by comparing measured radiant/velocity values for known showers (measured with higher precision photographic techniques) against individual radar meteoroid orbits. However, as will be seen in the results section, the mean values found from a large collection of radar measured orbits for each shower gives excellent agreement with velocity/radiants from the major showers measured using other techniques.

Our final remaining uncertainty relates to the magnitude of the deceleration correction to be applied to each measured orbit. Brown et al. (2004) used major showers as calibration points for CMOR data to compute a mean correction as a function of measured velocity and height—this CMOR-specific correction was applied to each echo having time of flight information. Fig. 4 shows this deceleration correction and compares it to others which have been used for radar data in the literature.

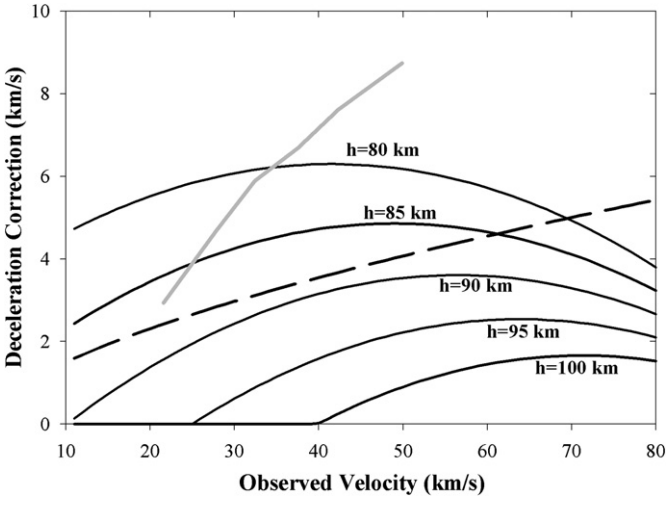

Fig. 4. The deceleration correction applied to/measured for radar meteor echoes. The solid curves represent the correction found empirically by Brown et al. (2004) for CMOR data as a function of height. The dashed curve is the correction applied to AMOR data as given by Baggaley et al. (1994) while the gray line is the deceleration values measured by the Harvard Radio Meteor Project as determined by Verniani (1973).

4. Shower search methodology

To detect a meteor shower in our data, two different techniques are used and then the results from each compared; only showers recognized by both are recorded as true showers. We begin by defining a meteor shower as a collection of meteoroids having similar velocity vectors at the Earth and which encounter the Earth continuously over a short (typically a few days, but in some cases as long as a month) period of time. The shower must show a significant clustering in the four measured quantities which uniquely define the orbit of a meteoroid encountering the Earth (such as the geocentric quantities α_g, δ_g, V_g, Ω) relative to the sporadic background. Note that since one node of the orbit must intersect the Earth, the orbit has $5 - 1 = 4$ degrees of freedom; hence only four quantities (orbital elements, geocentric quantities, state vectors, etc.) need be defined. Since the meteoroid stream has broadly similar orbital parameters across its cross-section, the geocentric radiant will move noticeably (with consistent $\Delta\alpha_g$, $\Delta\delta_g$,) over time in response to the changing heliocentric velocity vector of the Earth. This may be used as a further means to discriminate noise from true showers.

From this definition it follows that a meteor shower with unknown characteristics may be detected in a number of ways. In increasing order of detection sensitivity these are:

A) An enhancement in meteor rates over a set period of time without radiant or velocity information, provided the enhancement is large compared to the sporadic background recorded by the same system. This technique is used in defining showers from forward-scatter radio observations, for example (cf. Yrjola and Jenniskens, 1998)
B) An enhancement in rates from a particular radiant over a set period of time. This is the standard method used for visual meteor observations (Rendtel et al., 1995).
C) An enhancement in rates from a particular radiant, with particular velocity, over a set period of time. This is the most sensitive means of detecting weak showers (cf. Gartrell and Elford, 1975) and is the technique which allows association of orbital elements to be used in cluster searches.

Here we make use of approaches B and C as described below.

4.1. Single station shower identification

In the first approach, all echoes recorded from the main site (for each of the three frequencies) are used to "map" radiant activity over the entire sky in one degree solar longitude time bins. This mapping exploits the specular nature of all meteor echoes observed by the radar; each echo direction must be at right angles to the actual radiant. The range of possible radiant locations defines a great circle on the sky. When combined with the time of occurrence (and location of the radar) it is possible to map the apparent radiant activity in equatorial coordinates day-by-day. Details of the technique are given in Jones and Jones (2006). Fig. 5 shows a typical daily map with showers identified. Note that definitive shower association is not possible for any particular echo using this approach.

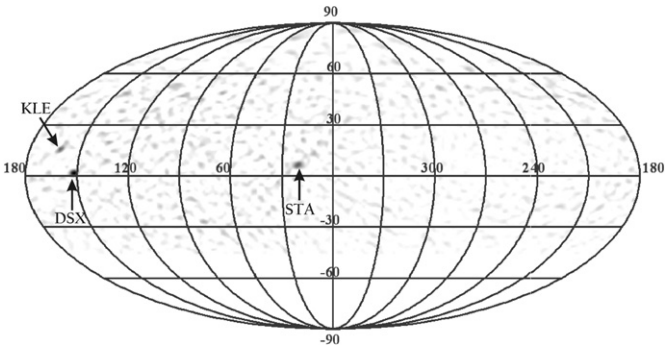

Fig. 5. A single station radiant activity map determined from 29.85 MHz data. The data are for $\lambda = 186°$ with all years between 1999–2006 combined. The coordinates are equatorial and the locations of three showers from our survey are shown for this particular solar longitude.

As our initial goal is to define those showers which recur year-to-year we have combined all data from all years into a single equivalent solar year binning echo data by solar longitude. Individual days in a given year having more than 4 h of radar downtime or where noticeable interference appeared on the radiant maps were removed from further analysis.

Radiant maps in equatorial coordinates were then constructed from these binned and combined data at all three frequencies. Data from 17.45 MHz suffers significant interference during the day which in turn produces artifacts in the radiant mapping process; we used 17.45 MHz data only as a check against the more reliable 29.85 and 38.15 MHz data.

Using these radiant maps, the strongest annual showers (Eta Aquariids, Geminids, Quadrantids) were easily visible. From a selection of these and several other known strong annual streams, we followed the full duration of each stream activity, noting the level at which the stream radiant merged into the sporadic background. This level, which was fairly stable from shower to shower, was then used to define our single station shower radiant strength significance cutoff relative to the sporadic background.

Each map for each degree of solar longitude was examined and all radiants having this significance cutoff value (or higher) were identified as a local maxima. This potential radiant list for a particular degree of solar longitude was then compared to the single degree bins before and after and any local maxima in those bins which were within two degrees in α_p and δ_p of the radiant position in the central solar longitude bin were recorded together as a possible linked radiant constituting a shower. These chains of linked radiants were then saved and those showing consistent positive drifts in α_p, and consistent drifts throughout their activity period in δ_p were identified. This final list was then manually examined to ensure no noise fluctuations identified as possible showers remained and the lists on 29.85 and 38.15 MHz compared for consistency. A final list of potential showers was then constructed of 47 probable streams at the end of this stage of the single station radiant analysis.

4.2. Orbit shower identification using wavelet transforms

Approach C from the earlier shower detection list involves searching for enhancements in the local density of orbital elements or equivalent. Since orbital elements transform nonlinearly with errors in measurement, we examine the equivalent set of geocentric parameters, such as α_g, δ_g, V_g, Ω—right ascension and declination of the geocentric radiant, velocity and time of meteor appearance; specification of these four quantities is equivalent to providing a complete set of orbital elements for a meteoroid impacting the Earth. We apply this search method to our individually measured orbits, numbering just over 2 million.

Following Galligan and Baggaley (2002a) we make use of the wavelet transform to search for enhancements relative to the sporadic background in the radiant and velocity space of our orbital dataset. The wavelet transform is well suited to searching for enhancements in datasets at different scale sizes (where some a priori knowledge of the shape of the enhancement is known) and has been applied to problems as diverse as asteroid family identification (Bendjoya et al., 1991) as well as astronomical image analysis (cf. Tiscareno et al., 2007). The 2D wavelet transform we use makes use of the Mexican Hat mother wavelet (which is well suited to point distributions having Gaussian shapes of enhancements; cf. Antoine, 2004):

$$W_c(x_0, y_0) = \frac{1}{\sqrt{2\pi}a} \int_{-\infty}^{+\infty}\int_{-\infty}^{+\infty} f(x,y)\left(2 - \frac{(x_0-x)^2+(y_0-y)^2}{a^2}\right) \times \exp\left[-\left(\frac{(x_0-x)^2+(y_0-y)^2}{2a^2}\right)\right] \mathrm{d}x\,\mathrm{d}y.$$

Here x, y are spatial coordinates on the sky (such as α_g, δ_g), a is the scale size (in degrees in our application) of the wavelet probe, $W_c(x_0, y_0)$ is the value of the wavelet coefficient at the test point and $f(x, y)$ is the distribution of geocentric radiants in our data. The design of the convolution is such that structure in $f(x, y)$ matching the probe size chosen for our wavelet will have large values of W_c. The convolution only has significant contributions from radiants that are roughly within one probe size of a particular test point. Note that the W_c values given in the present work ignore the leading $1/\sqrt{2\pi}$ term.

To further enhance the signal of weak showers in our orbital dataset, we structure our search to be equivalent to a 3D wavelet transform by first partitioning all our radiant data by velocity. This is done using bins of width comparable to our velocity measurement error of ∼10%; thus the bin centered at 33 km/s includes all radiants with measured time of flight velocities from 30–36 km/s. Finally, we divide all our orbital data temporally into one degree bins of solar longitude of time of occurrence and combine all years of data into 360 bins.

Since we do not know a priori what probe size will produce a maximum in W_c (and hence be a best fit probe size for a particular shower radiant), we compute wavelet coefficients for all velocity bins and each degree of solar longitude for discrete probe sizes of 1°, 2°, 3°, 4° and 8°. This number of probe size choices × velocity bins represents a total of 105 combinations of wavelet time series to be computed. As radiant positions for showers drift less in Sun-centered ecliptic coordinates, the final stage of searching for significant maxima in W_c is performed with all radiants transformed to $(\lambda - \lambda_0, \beta)$, where λ is the ecliptic longitude of the radiant, λ_0 the solar longitude at the time of the meteor echo and β is the ecliptic latitude of the radiant. For each degree of solar longitude, W_c is computed in steps of 0.5° of $\lambda - \lambda_0$ from 0° to 359.5° and from −40° to +90° in β.

From this map of W_c in a one degree bin of solar longitude, all W_c values are located which are apparent local maxima. These are defined by searching within any 2° region of a particular W_c value—if no points are found which have greater values of W_c then we identify $W_c(\lambda - \lambda_0, \beta)$ as a local maximum. Next, the median and standard deviation of $W_c(\lambda - \lambda_0, \beta)$ is computed over all degrees of solar longitude. Points more than 3σ above the median are discarded and the process iteratively repeated until no more points forming the median at that grid location lie outside the 3σ bounds. Local maxima more than 3σ above the final median estimate and where the density of radiants is above a minimum threshold determined through simulations to exceed that produced from a uniform background were selected for the next step in the search. The latter criteria (minimum density of radiants) was imposed to avoid selecting local maxima in the region of the antapex where radiant density is very low and hence a statistical fluctuation of only a few radiants in one position tends to produce false maxima.

These local maxima are then linked as potentially representing a single shower across individual solar longitude bins, provided they are separated by less than 2.5° in $(\lambda - \lambda_0, \beta)$ or less than 3.5° if separated by two degrees of solar longitude. These potential showers are further filtered by requiring one of the local maxima to be 10σ above the background. Single radiant points visible for only one solar longitude bin were only considered potential showers if the local maximum was 15σ above the background.

This process produced many duplicate "chains" of linked local maxima all from the same shower among the 105 combinations in the wavelet time series. To optimize the signal among these chains (i.e., to pick the best chain with the various combinations of probe size, velocity cut-off), the solar longitude bin of the maximum $W_c(\lambda - \lambda_0, \beta)$ was first used to refine the velocity of the potential shower. The $W_c(\lambda - \lambda_0, \beta)$ was recomputed using different centered velocity bins (still spanning 10% of the central velocity bin) with 1 km/s incrementing steps and a Gaussian fit performed on the distribution to identify the peak bin ($V_{g\,\max}$) and spread σ_g.

With a best estimate for the velocity of the shower from the previous step, the peak bin in velocity, $(\lambda - \lambda_0, \beta)$ and solar longitude was then used and a range of probe sizes (from 0.1°–20° at 0.1° intervals) applied to the maximum point. In general, this procedure produced a function showing a clear maximum, indicating the best choice of probe size for a particular radiant, $a_{\max}$. We found that most showers had similar-shaped probe size distributions of $W_c(\lambda - \lambda_0, \beta)$, usually with $a_{\max} = 3°$–4°. This is similar to the findings of Galligan and Baggaley (2002b) and suggests that this represent the size-scale of our measure-

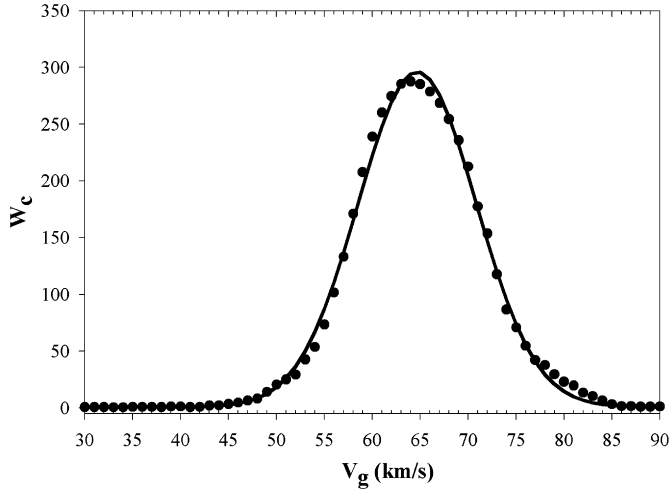

Fig. 6. The wavelet velocity fit to the Eta Aquariid shower. The individual circles represent the value of the wavelet coefficient centered at discrete 1 km/s intervals. Each measured bin represents the center of a velocity window having a width 10% of the center value. The solid line is a non-linear Gaussian fit to this distribution. The peak of the Gaussian fit is taken to be the best estimate for the wavelet shower velocity and the width of the Gaussian is the spread in the measured speeds.

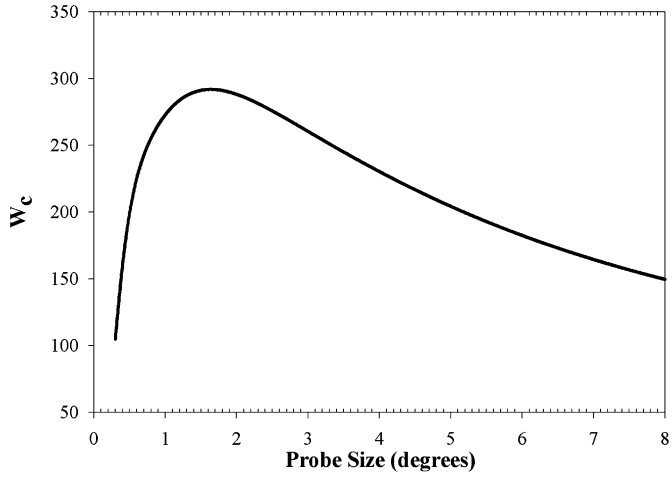

Fig. 7. Wavelet probe size fit to the Eta Aquariid shower for solar longitude 45°.

ment error, as opposed to an intrinsic physical spread for the radiants (in most cases).

Figs. 6 and 7 show this procedure in practice as applied to the Eta Aquariid shower.

From this velocity and probe size fit, the final set of shower measurements was made (from this optimal combination) using the wavelet transforms previously computed with integral probe sizes (1°, 2°, 3°, 4° and 8°) using the bins closest to this probe maximum. For each shower this produced a list of shower radiant locations as a function of solar longitude with measurement of the $W_c(\lambda - \lambda_0, \beta)$ as well as the number of standard deviations this $W_c(\lambda - \lambda_0, \beta)$ value was above the median background (for the entire year). A final check on each probable shower was performed to ensure that $\Delta\alpha > 0$ and $\Delta\delta$ as a function of solar longitude was consistent.

This set of wavelet maxima as a function of solar longitude was then used to further extract individual orbits from our dataset. We assume the distribution of radiants is Gaussian about the peak $W_c(\lambda - \lambda_0, \beta)$ for each solar longitude bin. From simulations we find that the relationship between the spread in a Gaussian source function and the probe size used for the Mexican Hat Wavelet is $\sigma = a_{\max}/\sqrt{3}$, a finding identical to that by Galligan (2000). It is interesting to note that our optimal probe sizes suggest widths of order ∼2° for most showers, an independent check on our estimate of our expected radiant measurement error. This is much larger than the spreads detected by photographic measurement of shower radiant sizes (e.g., Kresak and Porubcan, 1970) which suggest values typically of order 0.3°–1.6°; only the Taurids show higher dispersion in the photographic data which would be comparable to our measurement error.

From this relationship we extracted those orbits which were within $a_{\max}/\sqrt{3}$ degrees of the $W_c(\lambda - \lambda_0, \beta)$ maximum and which had V_g in the interval $V_{g\max} \pm \sigma_g$. These orbits represent the core of each stream—additional members could be added (particularly for the strong showers) by relaxing either or both of these constraints, but we chose here to sacrifice some orbit numbers to be certain of minimal sporadic contamination, even for minor streams.

A total of 45 streams were found in this second stage of the analysis to be in common with our first (single station) analysis.

5. Results

The results of the 45 streams identified in our analysis are given in Tables 3 and 4.

Table 3 summarizes measurements made from single station data alone—here 29.85 MHz values are chosen, though radiant drifts determined from 38.15 MHz single station analysis are generally comparable. The begin and end solar longitudes reflect the times when the showers merge below the sporadic background as described in Section 4.1. The relative intensity of single station activity (termed Z) is also given in the table—this is roughly proportional to the number of echoes contributing to the radiant "point" per degree of solar longitude. It is not related to the absolute flux as no corrections for mass dependence or collecting area have been performed—thus the relative strengths of different showers are not directly comparable. The activity profile for a particular shower, however, does reflect the relative change in flux to the mass limit of that particular stream.

The table also summarizes the radiant location at the time of maximum. Since single-station radiant mapping does not make use of velocity information directly, this is an apparent radiant location only—it does not have zenithal attraction, diurnal aberration or other corrections applied to provide true geocentric radiant coordinates. The radiant drift (per degree solar longitude) should be comparable to that measured with the wavelet analysis; note that the single station data has ∼4 times as much data on average per shower so the drift values here (particularly for weaker streams) may be more robust than the corresponding values obtained from the multi-station analysis. These drift values were computed in α_p, δ_p assuming a linear dependence on solar longitude. For showers of long duration (such as the South Delta Aquariids or the Taurids) this linear assumption is only

Table 3
Shower survey results from single station observations made at 29.85 MHz

IAU name or proposed	Three letter code	λ_{max}	λ_{begin}	λ_{end}	Max Z	α_{max}	δ_{max}	$\Delta\alpha$	$\pm\Delta\alpha$	$\Delta\delta$	$\pm\Delta\delta$
April Lyrids	lyr	32.5	30	34	36	271.9	33.5	0.78	0.16	−0.42	0.21
Daytime April Piscids	aps	32.5	30	36	26	9.4	10.9	0.90	0.08	0.37	0.05
Eta Aquariids	eta	44.5	33	64	277	336.2	−0.9	0.69	0.01	0.33	0.01
South Daytime May Arietids	sma	47.5	30	61	30	28.6	9.7	0.97	0.03	0.30	0.02
Northern Daytime Omega-Cetids	noc	47.5	30	59	29	8.7	19.3	0.97	0.03	0.31	0.01
Southern Daytime Omega-Cetids	oce	49.5	34	59	32	23.4	−3.2	0.90	0.03	0.43	0.02
Daytime Arietids	ari	76.5	65	93	255	41.9	25.4	0.63	0.02	0.19	0.01
Daytime Zeta Perseids	zpe	83.5	47	95	41	64.7	27.9	1.01	0.02	0.25	0.01
Southern June Aquilids	szc	80.5	78	81	28	304.7	−31.3	−0.25	0.34	0.46	0.16
Daytime Lambda Taurids	dlt	81.5	77	93	32	50.2	12.1	0.82	0.11	0.34	0.04
Epsilon Perseids	epr	95.5	92	107	24	57.8	37.4	0.77	0.08	0.42	0.06
Daytime Beta Taurids	bta	96.5	82	103	45	84.9	22.7	0.88	0.07	0.05	0.01
Epsilon Pegasids	epg	106.5	104	109	22	320.9	10.7	0.60	0.21	−0.36	0.26
Northern June Aquilids	nzc	108.5	85	114	29	314.5	−2.2	0.81	0.02	0.20	0.02
Beta Equuleids	beq	108.5	104	113	20	322.5	8.6	0.84	0.18	−0.45	0.19
Alpha Lacertids	ala	110.5	100	113	25	354.6	55.1	0.95	0.24	0.37	0.11
Psi Cassiopeids	pca	116.5	112	120	27	5.2	64.4	0.62	0.26	0.68	0.18
Alpha Capricornids	cap	124.5	102	130	36	304.1	−6.6	0.69	0.02	0.24	0.01
Southern Delta Aquariids	sda	125.5	115	155	356	339.4	−15.3	0.77	0.01	0.28	0.01
Piscis Austrinids	pau	125.5	121	138	26	347.7	−22.6	0.53	0.1	0.17	0.06
Southern Iota Aquariids	sia	129.5	125	149	22	332.5	−14	0.93	0.05	0.34	0.02
Daytime Xi Orionids	xri	131.5	116	138	19	102.9	18.6	0.81	0.06	−0.09	0.03
Northern Delta Aquariids	nda	137.5	131	159	22	345.2	2.2	0.70	0.03	0.33	0.01
Perseids	per	139.5	123	142	103	45.4	57.7	1.35	0.07	0.23	0.02
Northern Iota Aquariids	nia	167.5	113	182	33	2.7	7	0.84	0.01	0.33	0.01
Daytime Kappa Leonids	kle	178.5	164	189	40	159.1	18.2	0.63	0.03	−0.31	0.02
Daytime Sextantids	dsx	187.5	180	193	83	154.4	−0.1	0.69	0.02	−0.58	0.02
Southern Taurids	sta	191.5	166	236	56	27	8.6	0.82	0.01	0.25	0.01
October Draconids	dra	195.5	195	195	20	264	57.6	0.00	0	0.00	0
Orionids	ori	209.5	196	222	132	95.2	16	0.84	0.02	0.03	0.01
Northern Taurids	nta	223.5	201	236	31	52.7	22.9	0.90	0.02	0.24	0.01
Leonids	leo	236.5	230	238	82	154.5	21.1	0.51	0.15	−0.48	0.14
November Orionids	noo	247.5	226	256	78	90.4	16.2	0.74	0.01	−0.02	0.01
Geminids	gem	260.5	243	269	817	112.1	34	1.12	0.01	−0.16	0.01
December Monocerotids	mon	262.5	253	266	21	102.9	8.9	0.53	0.06	−0.05	0.05
Ursids	urs	270.5	270	270	29	212.5	75.1	0.00	0	0.00	0
Sigma Serpentids	sse	275.5	271	282	18	244.8	−3.7	0.74	0.08	−0.16	0.11
January Leonids	jle	280.5	278	284	42	145.3	25.4	0.99	0.1	−0.36	0.03
Omega Serpentids	oms	280.5	270	281	25	244.9	2.1	0.60	0.06	0.08	0.1
Quadrantids	qua	283.5	281	286	238	230.6	50.4	−0.01	0.32	0.38	0.32
Alpha Hydrids	ahy	290.5	280	294	17	131.1	−7.9	0.69	0.05	−0.19	0.03
Theta Coronae Borealids	tcb	296.5	294	300	24	227.4	41.2	1.57	0.17	−0.91	0.11
Lambda Bootids	lbo	295.5	283	299	27	218.8	45.7	1.36	0.13	−0.62	0.05
xi Coronae Borealids	xcb	295.5	291	303	18	245.9	32.2	0.69	0.15	0.05	0.11
Alpha Antilids	aan	313.5	308	321	24	159.9	−9.3	0.91	0.05	−0.38	0.06

The solar longitude of apparent activity maximum (λ_{max}), the start and end solar longitude of activity as defined in the text (λ_{begin} and λ_{end}, respectively) and the relative activity strength at maximum (Max Z) are shown for each shower.

an approximation; for these cases a somewhat better fit could be found by adopting a second order dependence in α_p, δ_p. All drift values were found by first rejecting points more than 3σ outside the confidence limits of the initial regression in both α_p, and δ_p. This procedure was repeated until all points were within 3σ of the best fit line in either α_p, or δ_p. Fig. 8 shows a typical single-station radiant drift plot from single station data from our data.

Table 4 summarizes the physical characteristics of the same radiants using the wavelet transform. The duration of the shower above the sporadic background (as outlined in Section 4.2) as well as the radiant position in geocentric equatorial coordinates (α_g and δ_g) are shown. The best fit velocity and standard deviation of the Gaussian fit are found using the procedure described in Section 4.2. The drifts in α_g, and δ_g were found using the same 3σ rejection technique as used with the single station fits. $W_{c\,max}$ for each shower and the best fit probe size are also provided. Fig. 9 shows a radiant drift plot from wavelet data.

From these wavelet fits, we have computed representative orbits using the observed radiants and best fit velocities from the wavelet transform maximum positions at the time of the shower maximum (as determined by the timing of $W_{c\,max}$). Table 5 shows these wavelet mean orbits.

Table 4
Shower survey results from orbit observations made at 29.85 MHz using wavelet analysis

IAU name or proposed	Three letter code	λ_{max}	λ_{begin}	λ_{end}	$W_{c\,max}$	$\alpha_{g\,max}$	$\delta_{g\,max}$	$\Delta\alpha$	$\pm\Delta\alpha$	$\Delta\delta$	$\pm\Delta\delta$	a_{max}	V_g (km/s)	σV_g
April Lyrids	lyr	32.5	31	33	26.8	272.3	32.6	1.50	0.06	−0.30	0.06	2	47.3	4.1
Daytime April Piscids	aps	24.5	16	33	18.1	3.8	5.5	0.90	0.04	0.39	0.03	4	28.9	3.4
Eta Aquariids	eta	45.5	35	59	285.2	338.0	−0.7	0.69	0.01	0.33	0.00	2	64.6	6.2
South Daytime May Arietids	sma	46.5	23	63	23.6	28.4	7.7	0.92	0.01	0.32	0.01	3	28.3	3.3
Northern Daytime Omega-Cetids	noc	45.5	16	58	38.4	9.0	17.3	0.95	0.01	0.36	0.01	4	36.8	4.1
Southern Daytime Omega-Cetids	oce	45.5	18	62	42.5	20.5	−6.1	0.93	0.01	0.44	0.01	3	36.9	3.9
Daytime Arietids	ari	74.5	64	88	169.8	41.7	23.6	0.60	0.02	0.19	0.01	3	39.1	4.2
Daytime Zeta Perseids	zpe	74.5	58	88	32.0	57.4	23.4	1.00	0.02	0.20	0.01	4	26.4	3.9
Southern June Aquilids	szc	80.5	78.0	82.0	31.1	304.7	−32.8	0.02	0.23	0.30	0.12	2	38.6	3.4
Daytime Lambda Taurids	dlt	85.5	70	98	19.2	56.7	11.5	0.82	0.02	0.27	0.01	4	36.4	3.7
Epsilon Perseids	epr	95.5	92.0	107.0	13.0	58.2	37.9	0.78	0.05	0.15	0.04	4	44.8	4.4
Daytime Beta Taurids	bta	93.5	90	100	25.8	82.0	20.0	0.89	0.08	0.04	0.05	4	27.4	3.1
Epsilon Pegasids	epg	105.5	104	106	17.2	326.3	14.7	1.50	0.40	0.45	0.38	4	29.9	3.2
Northern June Aquilids	nzc	101.5	77	117	44.8	310.4	−4.9	0.83	0.01	0.16	0.01	4	38.4	3.9
Beta Equuleids	beq	106.5	104	112	16.4	321.5	8.7	0.69	0.09	−0.28	0.14	3	31.6	3.1
Alpha Lacertids	ala	105.5	102	110	13.9	343	49.6	0.70	0.19	0.37	0.07	3	38.9	3.3
Psi Cassiopeids	pca	117.5	110	124	22.1	11.9	65.4	1.22	0.15	0.43	0.06	3	44	4.6
Alpha Capricornids	cap	123.5	116	128	19.9	302.9	−9.9	0.66	0.02	0.28	0.02	2	22.2	2.3
Southern Delta Aquariids	sda	126.5	115	145	342.4	341.0	−16.1	0.78	0.01	0.25	0.01	3	41.1	3.8
Piscis Austrinids	pau	126.5	125	131	11.0	347.9	−23.7	0.89	0.09	0.16	0.09	3	44.1	3.7
Southern Iota Aquariids	sia	129.5	128	133	11.5	332.9	−14.7	0.36	0.12	−0.14	0.07	3	30.5	3.1
Daytime Xi Orionids	xri	131.5	131	133	6.5	102.9	16.6	0.90	NA	−0.40	NA	3	45.4	4.2
Northern Delta Aquariids	nda	138.5	128	155	19.7	344.9	2.2	0.75	0.03	0.28	0.02	3	37.7	4.3
Perseids	per	139.5	134	142	74.5	46.9	56.9	1.23	0.09	0.27	0.07	3	62.1	7.2
Northern Iota Aquariids	nia	159.5	145	176	18.8	356.0	3.0	0.80	0.02	0.33	0.02	3	28.6	3.6
Daytime Kappa Leonids	kle	182.5	171	193	21.7	161.5	15.4	0.55	0.02	−0.26	0.02	2	43.3	4.5
Daytime Sextantids	dsx	186.5	174	194	61.9	154.6	−1.4	0.70	0.03	−0.51	0.01	3	31.84	3.3
Southern Taurids	sta	196.5	172	218	49.9	31.0	8.0	0.82	0.01	0.29	0.01	4	27.92	3.7
October Draconids	dra	195.5	195	195	24.4	261.7	54.8	0.00	0.00	0.00	0.00	2	19.7	2.3
Orionids	ori	207.5	198	221	96.3	94.7	15.5	0.78	0.01	0.03	0.01	3	66.4	6.3
Northern Taurids	nta	224.5	207	235	21.9	53.3	21.0	0.88	0.01	0.19	0.02	3	28.1	2.9
Leonids	leo	236.5	228	238	29.2	155.0	21.6	0.63	0.08	−0.27	0.06	2	69	6.8
November Orionids	noo	245.5	230	253	63.9	90.2	15.5	0.74	0.02	−0.06	0.01	3	43.5	3.9
Geminids	gem	261.5	244	267	568.0	112.8	32.1	1.10	0.02	−0.17	0.02	3	35	3.8
December Monocerotids	mon	261.5	252	264	21.3	102.6	8.1	0.63	0.03	−0.11	0.05	2	41.5	3.7
Ursids	urs	270.5	270	270	39.5	222.0	74.6	0.00	0.00	0.00	0.00	3	37.6	5.1
Sigma Serpentids	sse	275.5	261	279	26.0	242.8	−0.1	0.75	0.02	−0.14	0.03	4	42.67	4
January Leonids	jle	282.5	280	284	37.6	148.3	23.9	0.66	0.11	−0.14	0.05	2	52.7	4.4
Omega Serpentids	oms	275.5	271	279	16.5	242.7	0.5	0.76	0.05	0.11	0.18	2	38.9	3.4
Quadrantids	qua	283.5	279	285	237.5	231.7	48.5	0.72	0.05	−0.55	0.23	3	42	4
Alpha Hydrids	ahy	285.5	281	289	15.6	127.6	−7.9	0.65	0.07	−0.17	0.06	4	43.6	3.9
Theta Coronae Borealids	tcb	296.5	293	303	63.2	232.3	35.8	0.70	0.16	−0.06	0.09	8	38.66	4.5
Lambda Bootids	lbo	295.5	285	297	34.4	219.6	43.2	0.88	0.08	−0.69	0.03	4	41.75	4.2
xi Coronae Borealids	xcb	294.5	291	303	23.0	244.8	31.1	0.69	0.09	−0.11	0.08	4	44.25	4.3
Alpha Antilids	aan	315.5	299	320	30.7	162.7	−12.6	0.84	0.03	−0.36	0.03	4	44.75	4.3

The solar longitude of apparent activity maximum (λ_{max}), the start and end solar longitude of activity as defined in the text (λ_{begin} and λ_{end}, respectively), the relative wavelet coefficient at maximum ($W_{c\,max}$) and the best fit probe size for the wavelet transform (a_{max}) are shown for each shower.

As described in Section 4.2 we have also selected all meteoroid orbits in the core of the stream based on the position of the wavelet maximum/velocity in each solar longitude bin. While the radiant positions are well defined and agree with literature values in most cases (see Section 6), the velocity at the top of the atmosphere depends on the deceleration correction. The uncertainty in this correction is the main source of error in our mean orbit determinations To provide some estimate for this uncertainty, Table 6 shows the fit to each stream at the time of maximum using values determined from linear regression fits to all the orbital parameters and radiant positions of individually determined stream orbits at the time of shower maximum using our best fit deceleration correction. The orbit at the time of maximum as determined using our measured, in—atmosphere velocity (no deceleration correction) is also shown as well as the orbit determine using the velocity derived from the hybrid-Fresnel technique of Hocking (2000). The range in orbital parameters between these values provides a guide to the uncertainty of the measurements due to deceleration corrections alone.

Finally, using the fit to all orbits (with deceleration correction) as a function of solar longitude, the change in orbital parameters as a function of time (and associated error) were computed for each shower. Fig. 10 shows an example of the

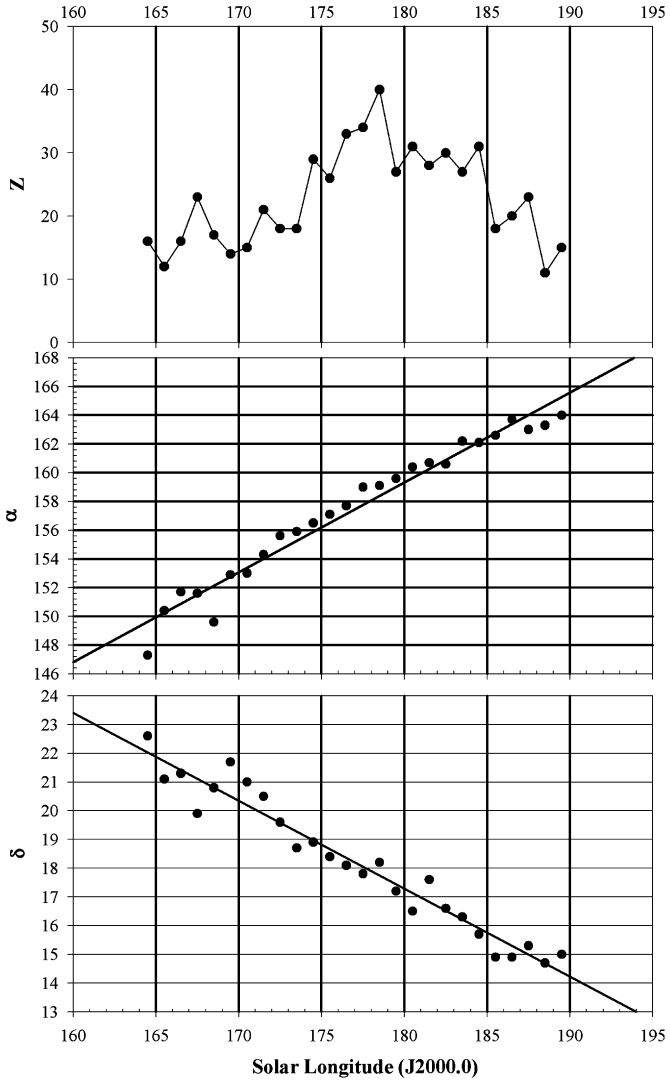

Fig. 8. A single station (29.85 MHz) activity plot (top) for the KLE shower. The radiant drift in right ascension (middle) and declination (bottom) are shown for the activity period of the shower. The solid lines represent the linear fits to these single station drifts.

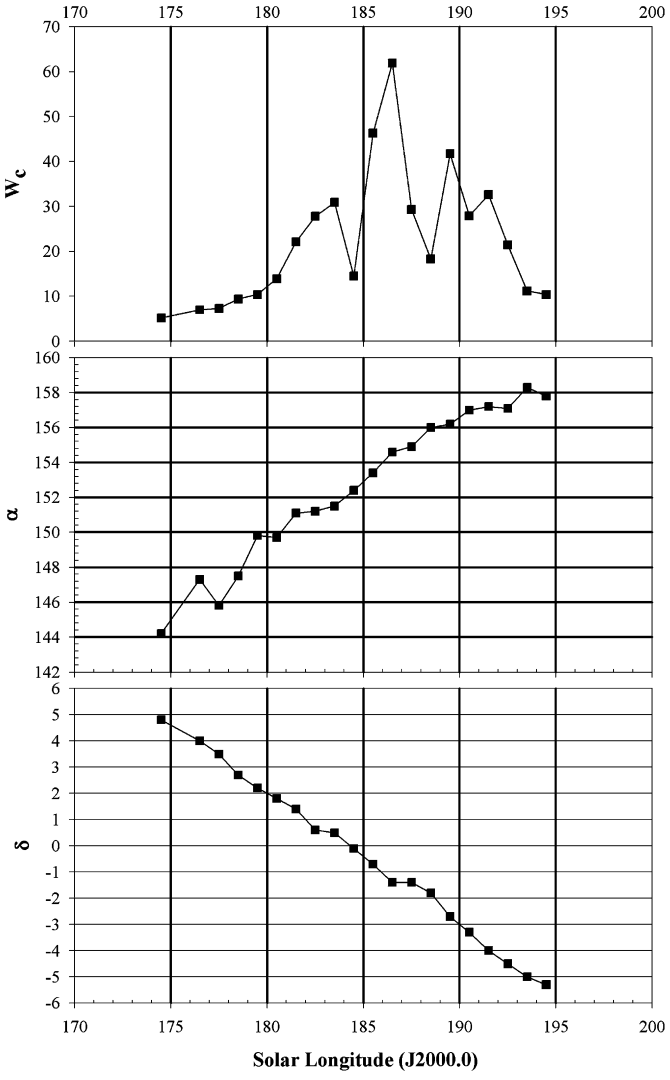

Fig. 9. A wavelet activity plot (top) for the DSX shower. The variations in strength at $\lambda = 184°$, 187° and 188° represent periods where data has been missed due to downtime in one of 2002–2006. The associated drift in right ascension (middle) and declination (bottom) are also shown.

change in orbital elements for a particular shower and associated fits. All quoted radiant and orbital values in the tables derived from these linear regression fits have been referenced to the solar longitude of the peak of the shower.

6. Discussion

Of the 45 showers in our list, a dozen are previously unreported or unrecognized in the literature. From the remainder, many have previously had only partial coverage of their activity period and/or have had limited measurements of their physical properties in earlier surveys. This is particularly true of the 14 daytime showers which have (in some cases) only been detected on one or two days of their activity by radar surveys made decades ago.

The closest survey in scope and technique to our own is that by Galligan and Baggaley (2002b) using the AMOR system. AMOR is sensitive to particles more than 100 times less massive than CMOR, so some intrinsic differences in quantities might be expected based on different evolutionary paths for different sized populations, but the overall measured parameters should be very similar. Note, in particular, that the AMOR deceleration corrections are quite different than those we employ and may produce of order 1–2 km/s differences in the initial geocentric velocity for the same data (see Fig. 4).

Of the six showers reported by Galligan and Baggaley (2002b), all have been detected in our survey as well. Table 7 compares their measurements to our own. The agreement is generally very good with essentially all the differences being within one standard deviation of the measurements. The two exceptions are the Eta Aquariids and Alpha Capricornids. Since the Eta Aquariids are a high inclination, near parabolic stream, the small difference in measured velocity (entirely ascribable to differences in the deceleration correction used) accounts largely for the variation in the elements between the two surveys.

Table 5
Representative mean orbits based on location and timing of the shower wavelet peaks

IAU name	Three letter code	a (AU)	e	q (AU)	Q (AU)	i (degs)	ω (degs)	Ω (degs)
April Lyrids	lyr	22.2	0.9589	0.913	43.5	80.7	215.8	32.3
Daytime April Piscids	aps	1.51	0.8309	0.256	2.8	4.7	50.1	24.7
Eta Aquariids	eta	7.07	0.924	0.537	13.6	162.9	91.6	45.1
South Daytime May Arietids	sma	1.51	0.8204	0.272	2.8	5.1	231.7	227.1
Northern Daytime Omega-Cetids	noc	1.58	0.9256	0.118	3.1	34.2	33.1	45.1
Southern Daytime Omega-Cetids	oce	1.72	0.9213	0.136	3.3	35.6	216.4	225.2
Daytime Arietids	ari	2.02	0.9593	0.082	4.0	24.8	28.7	75.0
Daytime Zeta Perseids	zpe	1.55	0.7841	0.335	2.8	3.8	58.4	75.0
Southern June Aquilids	szc	1.12	0.9433	0.064	2.2	56.0	158.6	260.4
Daytime Lambda Taurids	dlt	1.57	0.9337	0.104	3.0	23.2	210.8	1.7
Epsilon Perseids	epr	4.55	0.9714	0.13	9.0	63.0	39.7	96.0
Daytime Beta Taurids	bta	1.66	0.8042	0.325	3.0	3.6	238.3	277.0
Epsilon Pegasids	epg	0.757	0.7711	0.173	1.3	55.4	334.9	105.2
Northern June Aquilids	nzc	1.71	0.9356	0.11	3.3	39.4	327.7	101.3
Beta Equuleids	beq	0.887	0.8164	0.163	1.6	49.7	330.3	106.2
Alpha Lacertids	ala	1.089	0.0799	1.002	1.2	81.1	217.1	105.3
Psi Cassiopeids	pca	2.14	0.5623	0.934	3.3	82.9	140.8	117.7
Alpha Capricornids	cap	2.35	0.75	0.586	4.1	7.3	269.2	123.3
Southern Delta Aquariids	sda	2.38	0.9726	0.065	4.7	30.9	153.9	306.2
Piscis Austrinids	pau	3.12	0.9611	0.122	6.1	64.1	142.8	306.2
Southern Iota Aquariids	sia	1.546	0.8587	0.218	2.9	5.3	134.3	309.1
Daytime Xi Orionids	xri	7	0.9932	0.048	13.9	33.2	204.1	311.3
Northern Delta Aquariids	nda	1.81	0.9464	0.097	3.5	24.1	329.3	138.6
Perseids	per	−6.4	1.15	0.963	inf	116.2	155.1	139.8
Northern Iota Aquariids	nia	1.52	0.825	0.266	2.8	5.7	309.0	158.8
Daytime Kappa Leonids	kle	5.92	0.9853	0.087	11.8	24.8	32.8	182.6
Daytime Sextantids	dsx	1.27	0.855	0.184	2.4	20.7	219.6	2.6
Southern Taurids	sta	1.67	0.8144	0.31	3.0	5.4	122.5	16.0
October Draconids	dra	2.89	0.6561	0.995	4.8	30.3	171.9	196.6
Orionids	ori	9.71	0.9385	0.597	18.8	163.6	80.1	27.0
Northern Taurids	nta	2.06	0.8283	0.354	3.8	2.3	294.8	223.8
Leonids	leo	4.22	0.7674	0.982	7.5	161.5	170.3	236.2
November Orionids	noo	11.8	0.9917	0.098	23.6	26.6	144.1	65.1
Geminids	gem	1.416	0.904	0.136	2.7	24.0	324.6	261.3
December Monocerotids	mon	22.3	0.9913	0.194	44.0	34.4	127.9	81.3
Ursids	urs	−10.3	1.09	0.948	inf	57.3	201.6	270.8
Sigma Serpentids	sse	1.92	0.9168	0.16	3.7	64.0	41.3	275.9
January Leonids	jle	6.3	0.9913	0.055	12.6	109.3	333.7	282.0
Omega Serpentids	oms	1.37	0.88	0.164	2.6	56.5	38.8	275.9
Quadrantids	qua	3.7	0.7367	0.975	6.4	72.5	168.5	283.2
Alpha Hydrids	ahy	12.7	0.9774	0.287	25.1	57.1	115.6	105.0
Theta Coronae Borealids	tcb	1.108	0.1662	0.924	1.3	77.0	124.9	296.5
Lambda Bootids	lbo	1.49	0.3579	0.956	2.0	79.3	206.6	295.4
xi Coronae Borealids	xcb	2.34	0.6509	0.817	3.9	79.6	124.7	294.5
Alpha Antilids	aan	2.47	0.9443	0.138	4.8	63.5	140.5	135.5

The case of the Alpha Capricornids is less clear. Both surveys suffer from small number statistics, but the difference in radiant position, in particular in α_g, is very large. Fig. 11 shows the radiant drift and in α_g and δ_g for the Alpha Capricornids from our data as well as the location of maximum for AMOR from Galligan and Baggaley (2002b) and from several other literature sources. While δ_g is consistent to within a degree between all literature values and CMOR/AMOR results, the α_g value from AMOR seems significantly different from other sources and CMOR. It would seem probable that either the AMOR measurements are less accurate than for the other showers (perhaps due to small numbers of orbits in the means) or the smaller particle sizes detected by AMOR have significantly different orbits than the larger meteoroids detected by CMOR/photographic/video data.

The location of all shower radiants at the time of their respective maximum in Sun-centered coordinates $(\lambda - \lambda_0, \beta)$ is shown in Fig. 12. The location and size of the principle sporadic sources (Jones and Brown, 1993) are also given. It is clear that the majority of showers (∼90%) are associated with one of the six major sporadic sources. This is suggestive that the dispersal of typical showers as seen at the Earth feeds the sporadic sources. It may also hint that the typical orbits at the Earth produced by debris released from meteoroid parent objects through encounter/orbital/evolutionary selection effects are confined to the regions outlined by the sporadic sources.

Table 6
Shower orbits using deceleration corrected velocities (1st row) raw (observed) mean velocities (2nd row) and velocities determined from the hybrid-Fresnel technique (3rd row) of Hocking (2000)

IAU name	Three letter code	a (AU)	e	q (AU)	Q (AU)	i (degs)	ω (degs)	Ω (degs)	V_g (km/s)	N_{orbits}
April Lyrids	lyr	25.2	0.9637	0.915	49.4	80.4	215.4	32.5	47.1	26
		6.8	0.8650	0.912	12.7	79.2	216.9	32.3	45.7	
		−287.0	1.0032	0.918	−574.9	81.1	214.3	32.3	47.8	
Daytime April Piscids	aps	1.5	0.8327	0.256	2.8	5.0	50.2	24.5	29.2	397
		1.3	0.7900	0.280	2.4	4.5	50.7	24.8	26.7	
		1.4	0.8147	0.267	2.6	4.9	50.5	24.8	28.0	
Eta Aquariids	eta	5.7	0.9068	0.533	10.9	163.0	89.6	45.5	64.0	1784
		2.8	0.8231	0.486	5.0	162.3	81.5	45.1	62.1	
		19.7	0.9713	0.564	38.8	163.2	96.0	45.1	65.7	
South Daytime May Arietids	sma	1.6	0.8183	0.286	2.9	5.4	233.7	226.5	28.2	583
		1.3	0.7790	0.297	2.4	4.4	232.3	227.1	26.2	
		1.4	0.8028	0.285	2.6	4.9	232.2	227.1	27.3	
Northern Daytime Omega-Cetids	noc	1.5	0.9216	0.115	2.8	35.7	32.0	45.5	36.6	1256
		1.3	0.9016	0.131	2.5	29.9	33.4	45.1	34.5	
		1.5	0.9166	0.123	2.8	32.4	33.2	45.1	35.9	
Southern Daytime Omega-Cetids	oce	1.6	0.9197	0.132	3.2	35.4	215.4	225.5	36.8	837
		1.5	0.8972	0.150	2.8	31.4	216.8	225.2	34.7	
		1.7	0.9154	0.140	3.2	34.1	216.7	225.2	36.3	
Daytime Arietids	ari	2.2	0.9597	0.088	4.3	25.1	29.8	74.5	39.3	2142
		1.7	0.9430	0.096	3.3	21.4	30.0	75.0	37.2	
		2.1	0.9609	0.083	4.2	24.6	29.0	75.0	39.3	
Daytime Zeta Perseids	ape	1.6	0.7896	0.335	2.9	4.3	58.7	74.5	26.7	843
		1.5	0.7628	0.349	2.6	3.7	58.9	75.0	25.5	
		1.7	0.8030	0.328	3.0	4.1	58.7	75.0	27.3	
Southern June Aquilids	szc	1.1	0.9400	0.065	2.1	57.0	158.7	260.5	38.4	65
		1.0	0.9278	0.071	1.9	47.4	158.9	260.5	35.8	
		1.0	0.9278	0.071	1.9	47.4	158.9	260.5	35.8	
Daytime lambda Taurids	dlt	1.6	0.9316	0.108	3.1	23.5	211.5	265.5	36.5	406
		1.4	0.9117	0.120	2.6	20.2	211.9	265.5	34.2	
		1.6	0.9317	0.107	3.0	22.8	211.2	265.5	36.2	
Epsilon Perseids	epr	3.9	0.9688	0.123	7.8	64.9	38.0	95.5	44.9	203
		2.3	0.9468	0.124	4.5	56.9	36.4	95.5	42.1	
		2.9	0.9568	0.123	5.6	59.8	37.1	95.5	43.2	
Daytime Beta Taurids	bta	1.9	0.8117	0.357	3.4	3.6	243.3	273.5	27.5	288
		1.8	0.7874	0.377	3.2	3.5	244.7	274.1	26.4	
		2.1	0.8244	0.361	3.7	3.6	244.7	274.1	28.2	
Epsilon Pegasids	epg	0.8	0.7664	0.176	1.3	55.1	334.4	85.5	29.8	62
		0.7	0.7675	0.173	1.3	52.5	335.7	105.3	29.7	
		0.7	0.7675	0.173	1.3	52.5	335.7	105.3	29.7	
Northern June Aquilids	nzc	1.6	0.9306	0.110	3.1	40.0	327.4	101.5	38.2	1377
		1.4	0.9158	0.121	2.8	34.4	327.4	101.4	36.2	
		1.6	0.9279	0.115	3.1	37.1	327.5	101.4	37.5	
Beta Equuleids	beq	0.9	0.8252	0.153	1.6	48.5	331.5	106.5	31.5	89
		0.8	0.8065	0.159	1.5	45.2	332.8	106.2	29.6	
		0.8	0.8144	0.156	1.5	47.8	332.4	106.2	30.5	
alpha Lacertids	ala	1.1	0.0791	0.981	1.1	81.8	240.2	105.5	39.0	66
		1.0	0.0835	0.873	1.0	76.5	326.6	105.3	35.8	
		1.0	0.0777	0.885	1.0	76.8	323.4	105.3	36.0	
Psi Cassiopeids	pca	2.2	0.5710	0.949	3.5	83.1	143.9	117.5	44.2	175
		1.5	0.4017	0.916	2.1	79.2	131.0	117.7	40.9	
		1.6	0.4297	0.921	2.3	80.0	133.4	117.7	39.6	
Alpha Capricornids	cap	2.3	0.7501	0.583	4.1	7.2	269.6	123.5	22.2	145
		2.2	0.7295	0.593	3.8	7.0	269.2	123.3	21.6	
		2.5	0.7720	0.579	4.5	7.5	269.2	123.3	22.8	
Southern Delta Aquariids	sda	2.3	0.9711	0.067	4.5	31.4	154.0	306.5	41.0	4722
		1.8	0.9573	0.075	3.4	26.1	153.4	306.2	38.8	
		1.9	0.9636	0.071	3.8	28.2	153.6	306.2	39.8	
Piscis Austrinids	pau	4.7	0.9741	0.121	9.2	65.0	141.8	306.5	45.2	91
		2.5	0.9513	0.120	4.8	61.3	144.0	306.2	42.9	
		2.5	0.9521	0.120	4.9	61.5	143.9	306.2	42.9	

Table 6 (*continued*)

IAU name	Three letter code	a (AU)	e	q (AU)	Q (AU)	i (degs)	ω (degs)	Ω (degs)	V_g (km/s)	N_{orbits}
Southern Iota Aquariids	sia	1.8	0.8593	0.249	3.3	5.0	129.3	309.5	30.5	353
		1.8	0.8603	0.245	3.3	4.7	129.8	309.1	28.3	
		1.5	0.8285	0.260	2.8	4.9	129.9	309.1	28.8	
Daytime Xi Orionids	xri	4.0	0.9895	0.042	8.0	34.8	201.8	311.5	44.9	204
		2.5	0.9792	0.052	4.9	27.5	203.4	311.3	42.2	
		3.0	0.9839	0.047	5.9	29.4	202.8	311.3	43.2	
Northern Delta Aquariids	nda	1.7	0.9452	0.092	3.3	25.2	330.9	138.5	37.5	460
		1.5	0.9229	0.112	2.8	20.9	328.5	138.6	35.4	
		1.6	0.9324	0.107	3.0	22.0	328.7	138.6	37.3	
Perseids	per	−6.0	1.1592	0.954	−12.9	115.4	152.6	139.5	61.8	361
		−106.5	1.0090	0.958	−214.0	115.2	153.1	139.8	60.4	
		61.2	0.9844	0.957	121.5	115.0	152.7	139.8	60.1	
Northern Iota Aquariids	nia	1.6	0.8238	0.280	2.9	5.5	307.1	159.5	28.5	509
		1.4	0.7932	0.281	2.4	5.6	309.2	158.9	26.9	
		1.4	0.8094	0.274	2.6	5.8	309.0	158.9	27.7	
Daytime Kappa Leonids	kle	8.0	0.9885	0.092	15.9	25.6	33.8	182.5	43.6	208
		3.3	0.9700	0.099	6.5	22.7	33.9	182.6	41.3	
		6.3	0.9861	0.088	12.5	25.7	33.1	182.6	43.4	
Daytime Sextantids	dsx	1.1	0.8603	0.147	2.0	23.2	212.2	6.5	31.5	556
		1.0	0.8336	0.168	1.8	20.4	213.7	6.5	29.7	
		1.1	0.8558	0.153	2.0	22.1	213.2	6.5	31.2	
Southern Taurids	sta	1.7	0.8171	0.319	3.2	5.1	121.1	16.5	28.0	2684
		1.6	0.7953	0.321	2.8	5.1	122.2	16.0	26.9	
		1.6	0.8064	0.314	2.9	5.2	122.4	16.0	27.5	
October Draconids	dra	3.0	0.6690	0.995	5.0	30.3	172.1	195.5	19.9	20
		2.9	0.6624	0.995	4.9	30.2	172.1	195.6	19.8	
		3.1	0.6782	0.995	5.2	30.5	172.1	195.6	20.0	
Orionids	ori	9.1	0.9377	0.565	17.6	163.2	84.8	207.5	65.7	1297
		3.2	0.8303	0.550	5.9	163.2	89.3	27.0	64.0	
		22.4	0.9728	0.610	44.2	164.0	77.6	27.0	67.0	
Northern Taurids	nta	2.1	0.8299	0.365	3.9	2.5	293.2	16.5	28.0	470
		1.8	0.7995	0.364	3.3	2.1	295.1	223.8	26.9	
		1.9	0.8171	0.356	3.5	2.2	295.2	223.8	27.7	
Leonids	leo	3.7	0.7366	0.983	6.5	161.7	171.2	236.5	68.6	126
		2.4	0.5883	0.981	3.8	161.2	168.1	236.2	66.9	
		11.9	0.9177	0.983	22.9	161.9	171.1	236.2	70.7	
November Orionids	noo	16.3	0.9935	0.106	32.5	26.6	142.5	65.5	43.4	1097
		3.9	0.9715	0.095	7.7	23.6	143.3	65.1	41.0	
		5.7	0.9820	0.088	11.4	25.2	143.8	65.1	42.3	
Geminids	gem	1.4	0.8996	0.138	2.6	23.6	324.7	261.5	34.7	4384
		1.2	0.8717	0.154	2.2	20.9	324.3	261.3	32.4	
		1.2	0.8805	0.148	2.3	21.7	324.5	261.3	33.0	
December Monocerotids	mon	21.2	0.9906	0.200	42.2	34.5	127.0	81.5	41.4	138
		4.6	0.9558	0.203	9.0	31.2	128.6	81.3	39.0	
		7.7	0.9746	0.196	15.2	32.8	128.5	81.3	40.4	
Ursids	urs	−11.7	1.0811	0.947	−24.3	57.5	202.1	270.5	37.4	71
		−224.4	1.0042	0.948	−449.7	56.2	202.0	270.8	36.3	
		11.6	0.9180	0.947	22.2	54.9	202.8	270.8	34.9	
Sigma Serpentids	sse	2.0	0.9216	0.157	3.9	62.4	41.1	275.5	42.6	540
		1.5	0.8942	0.157	2.8	57.8	38.7	275.9	39.9	
		1.8	0.9118	0.158	3.4	62.5	40.5	275.9	42.0	
January Leonids	jle	8.7	0.9939	0.053	17.4	105.3	333.9	282.5	52.5	138
		3.0	0.7567	0.009	5.2	99.5	336.7	282.0	50.1	
		4.3	0.9877	0.053	8.5	104.5	334.8	282.0	51.6	
Omega Serpentids	ose	1.6	0.8999	0.156	3.0	56.8	38.8	275.5	40.0	60
		1.2	0.8651	0.168	2.3	53.1	38.1	275.9	37.4	
		1.7	0.9034	0.165	3.2	62.7	41.1	275.9	41.6	
Quadrantids	qua	3.4	0.7179	0.973	5.9	72.7	167.1	283.5	42.0	881
		2.5	0.6108	0.974	4.0	70.3	167.4	283.2	39.9	
		2.6	0.6243	0.974	4.2	70.6	167.5	283.2	40.2	
Alpha Hydrids	ahy	8.7	0.9677	0.282	17.2	58.5	116.9	105.5	43.6	193
		4.5	0.9363	0.286	8.7	54.2	117.8	105.0	41.5	
		5.9	0.9513	0.286	11.5	55.4	117.1	105.0	42.6	

(*continued on next page*)

Table 6 (*continued*)

IAU name	Three letter code	a (AU)	e	q (AU)	Q (AU)	i (degs)	ω (degs)	Ω (degs)	V_g (km/s)	N_{orbits}
Theta Coronae Borealids	tcb	1.1	0.2080	0.884	1.3	77.1	112.2	296.5	38.6	1123
		1.0	0.1216	0.852	1.1	72.7	76.5	296.5	35.7	
		1.0	0.1232	0.880	1.1	74.0	92.1	296.5	36.5	
Lambda Bootids	lbo	1.5	0.3680	0.952	2.1	79.0	208.8	295.5	41.6	354
		1.2	0.2211	0.945	1.5	75.6	218.5	295.4	38.7	
		1.3	0.2539	0.949	1.6	76.7	214.1	295.4	39.5	
xi Coronae Borealids	xcb	2.6	0.6884	0.805	4.4	79.4	123.1	294.5	44.5	185
		1.8	0.5500	0.797	2.7	76.9	117.7	294.5	41.9	
		1.8	0.5595	0.799	2.8	77.2	118.5	294.5	42.1	
Alpha Antilids	aan	2.6	0.9481	0.136	5.1	62.1	140.5	135.5	44.3	565
		1.8	0.9251	0.138	3.5	58.1	142.3	135.5	41.9	
		1.9	0.9287	0.137	3.7	59.0	142.0	135.5	42.3	

The orbits in all cases are found by least squares fitting to the orbital elements for all individually selected orbits as a function of solar longitude and are then referenced to the solar longitude of the peak. The number of selected orbits for each shower is given in the last column (N_{orbits}). Angular elements are all J2000.0.

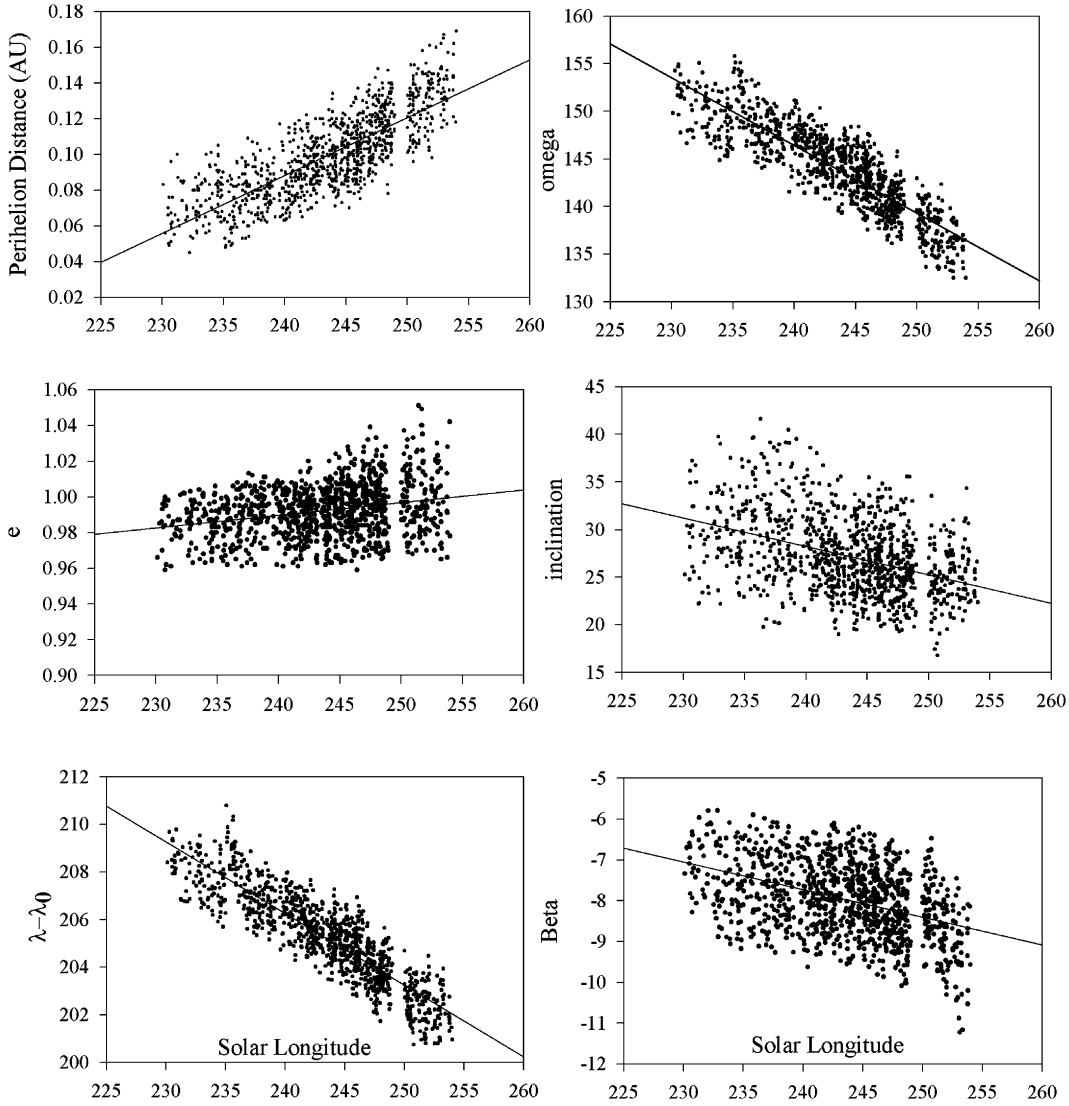

Fig. 10. The variation in orbital elements as a function of solar longitude for the MON shower. Each point represents one orbit selected according to the criteria discussed in the text. The (assumed) linear fits to each orbital element are also shown.

Many showers have asteroidal-type orbits (based on a Tisserand value >3.0 for the mean stream orbit). However, as emphasized by Wiegert (2007), this does not necessarily imply asteroidal parent bodies. Small meteoroids in our size regime

Table 7
Shower measurements made with AMOR as compared to CMOR

Shower	λ_{max} (deg)	q (AU)	e	i (deg)	ω (deg)	V_g (km/s)	α_{max} (deg)	δ_{max} (deg)	$\Delta\alpha$ (deg)	$\Delta\delta$ (deg)	a_{max} (deg)	N_{orb}
CAP	122.3	0.550	0.768	7.7	273.3	23.4	306.7	−9.3	0.91	0.25	3	269
	123.5	**0.578**	**0.748**	**7.1**	**270.4**	**22.3**	**302.6**	**−10.4**	**0.66**	**0.27**	**2**	**145**
SDA	127.2	0.067	0.966	30.8	154.5	40.2	340.4	−16.3	0.73	0.26	3	2413
	126.5	**0.068**	**0.970**	**31.1**	**153.6**	**40.9**	**341.7**	**−16.0**	**0.78**	**0.28**	**3**	**4722**
AAN	313.1	0.143	0.92	64.3	141.9	42.7	162.1	−13.3	0.68	−0.16	3	327
	315.5	**0.136**	**0.948**	**62.6**	**140.6**	**44.3**	**160.6**	**−11.4**	**0.83**	**−0.37**	**4**	**565**
OCE	45	0.133	0.916	37.1	214.9	36.5	19	−7	0.8	0.38	3	970
	45.5	**0.132**	**0.919**	**35.4**	**215.4**	**36.8**	**19.7**	**−6.3**	**0.93**	**0.44**	**3**	**837**
DSX	186.1	0.151	0.855	23.1	212.5	31.2	154.5	−1.5	0.84	−0.43	3	410
	186.5	**0.147**	**0.861**	**23**	**212.3**	**31.5**	**153.8**	**−1**	**0.7**	**−0.51**	**3**	**556**
ETA	45.4	0.55	0.939	165.3	93.1	65.1	339.1	−1.5	0.73	0.31	2	942
	45.5	**0.533**	**0.907**	**163.0**	**89.6**	**64.0**	**338.1**	**−0.8**	**0.69**	**0.33**	**2**	**1784**

Parameters which show daily motion are corrected to the time of maximum as determined from AMOR data for ease of comparison. All angular elements are J2000.0—symbols are defined in the text. AMOR data are given in the first row and CMOR (in bold) in the second row for each shower. Shower three letter codes are given in Tables 3 and 4.

are subject to strong Poynting–Robertson drag effects which are particularly pronounced for orbits with small q. In our sample, more than 1/3rd of all streams have $q < 0.15$ AU—such meteoroids may begin in highly eccentric, relatively large orbits and quickly lose energy over timescales less than one precession cycle. This may account for the peculiar orbital characteristics of many of the streams in our survey. It is likely many of these streams are linked to recently deceased sungrazing comets, sungrazers being a common end-state for comets with $q < 2$ AU (Bailey et al., 1992). These streams may therefore be the "smoking" gun for many now defunct sungrazers and might also suggest orbital elements for additional unrecognized sungrazing groups (cf. Sekanina and Chodas, 2005).

We find a total of 0.8% of all orbits identifiable with the core of our streams as previously defined. Relaxing the association to all meteoroids within 5° of a particular shower radiant location (but still being having V_g in the interval $V_{g\,max} \pm \sigma_g$) we find a more realistic estimate of the fraction of the meteoroid population in streams at $\sim 10^{-7}$ kg to be 3.4%. While subjective relaxation of other criteria (such as the velocity cut) may raise this slightly further, it is clear that at these masses <10% of the total population is in a recognizable stream. According to Hughes (1990) sporadic meteoroids completely dominate the flux at these sizes, in agreement with our findings.

Some additional notes related to specific showers:

Daytime April Piscids (APS). This shower has been linked with the South Daytime May Arietids (SMA), as well as the North (NIA) and South Iota Aquariids (SIA) by Wiegert (2007). Each stream represents a different intersection point from a single apsidally precessed original orbit. The proximity of the APS to SMA radiants has led to confusion between the two in previous studies (e.g., Kronk, 1988, who recognized the potential link to the NIA shower, but confuses the APS and SMA, which last much longer).

Daytime Arietids (ARI). This strongest of the daylight streams (and 5th most active of all streams in our analysis) was previously analyzed by Campbell-Brown (2004) based on three

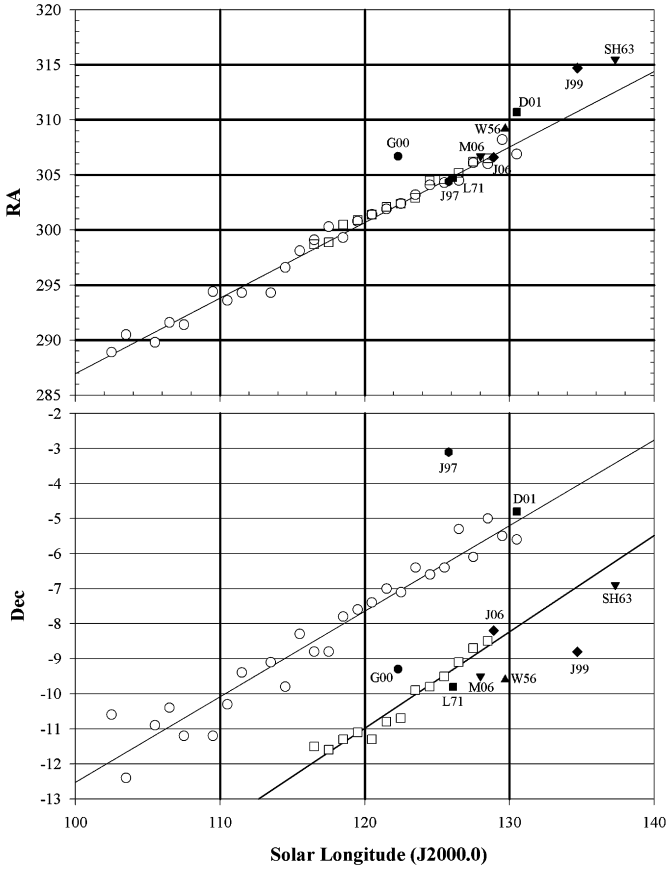

Fig. 11. Radiant drift for the CAP shower. The open circles represent radiant position measured from single station data while the open squares are the radiant fits from the wavelet transform. The systematic shift in declination between single station and wavelet measurements reflects the inclusion of zenithal attraction correction for the geocentric radiants for the latter. The individual solid symbols represent the location of maximum for the shower. Abbreviations: G00 (Galligan, 2000); J97 (Jopek and Froeschle, 1997); L71 (Lindblad, 1971); M06 (Molau, 2006); J06 (Jenniskens, 2006); W56 (Wright et al., 1956); D01 (Dutch Meteor Society Photographic Orbits—Betlem et al., 1995); J99 (Jopek et al., 1999); SH65 (Southworth and Hawkins, 1963).

years of CMOR data. The out of atmosphere velocity found in the first analysis (uncorrected for deceleration) was 37.6 km/s, which compares favorably with our raw, observed velocity of 37.3 km/s based on just over twice as much data. The radiant position in the original analysis was apparent as it was derived from single station analysis, with a value for δ several degrees higher than our geocentric values, reflecting the lack of zenith attraction correction. The stream is undoubtedly related to the Marsden group of sungrazers as discussed recently by Sekanina and Chodas (2005).

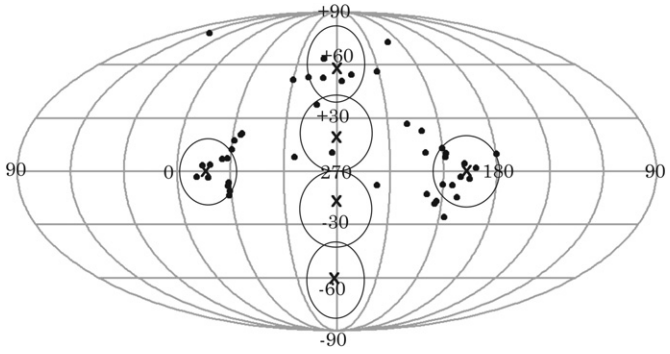

Fig. 12. Location of the radiant determined from wavelet analysis at the time of maximum for each shower detected in the CMOR survey in Sun-centered radiant coordinates. The location of the six major sporadic sources from Jones and Brown (1993) is also given.

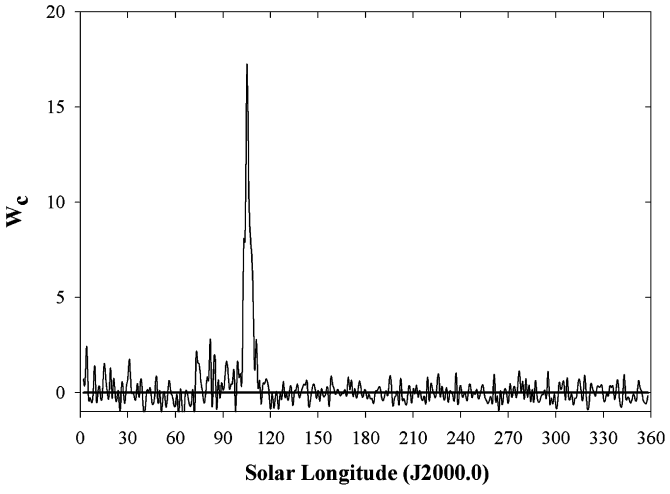

Fig. 13. The wavelet coefficient measured at the Sun-centered radiant location at the time of the peak of the EPG shower determined throughout the year.

Southern June Aquilids (SZC). This is among the weaker showers detected in our survey. Previous literature has identified a number of radiants in the Sagittarius region at this time of the year (cf. Rendtel et al., 1995; Kronk, 1988; Jenniskens, 2006). The literature references most consistent with a linkage with the CMOR-measured stream are summarized in Table 8. In particular, the recent video survey of Molau (2006) show this shower with very nearly the same velocity and radiant location as in the present survey. One possible explanation for the paucity of literature references lies in the unusual mass distribution of CMOR observed meteors from this stream—the average stream member is near +8, while most other streams and our orbit dataset as a whole are one full magnitude brighter on average. This appears to be a real effect and suggests a strong preponderance of small particles in the shower. Though the shower is weak in our data, we note that the deep southern declination of the radiant means it has ∼10 times less daily collecting area coverage as a radiant near the north equatorial pole.

Epsilon Perseids (EPR). This is a newly recognized weak shower occurring in late June/early July. The stream's orbit is almost identical to that of 96P/Machholz (Wiegert, 2007), differing only slightly in the argument of perihelion. This stream is the newest and perhaps the youngest of the proposed Machholz complex (Ohtsuka et al., 2003).

Epsilon Pegasids (EPG). This shower is also very weak, but shows up clearly in wavelet analysis (Fig. 13). Molau (2006) lists a probable detection of the stream near the peak of the shower, quoting a radiant less than 3° from the CMOR radiant position, though it is based on 9 video meteors only. The orbit is quite unusual—it is an Aten-type but with an inclination of 55°. Again, the effects of Poynting–Robertson are likely at work for this small-q stream (Wiegert, 2007) which probably was released from a Jupiter Family comet. The large inclination suggests that the shower is not an artifact of unusually high collision probabilities alone.

Northern June Aquilids (NZC). Though listed by Jenniskens (2006) as the northern twin to the SZC, as identified here the inclinations and perihelia are sufficiently distinct to suggest they are not related. This relatively strong stream has no obvious immediate parent, but its small-q indicates fast evolution under PR-drag generically suggestive of a Jupiter-family comet origin.

Alpha Lacertids (ALA). This stream is unusual for having a nearly circular orbit with an a ∼1 AU but high inclination. Both Sekanina (1976) and Kashcheyev and Lebedinets (1967) record

Table 8
Literature linkages and details for the Southern June Aquilids (SZC)

Reference	λ_{max} (°)	α (°)	δ (°)	V_g (km/s)	$\Delta\alpha$	$\Delta\delta$	a (AU)	e	q (AU)	i (°)	ω (°)	Ω (°)	Comments
Gartrell and Elford (1975)	79.7	297.8	−33.9	33.2			1.15	0.9	0.11	33.5	152	259	Based on 4 radar orbits
Weiss (1960)	80	304.8	−34.8										
Molau (2006)	80	304	−34	40.5									Based on 36 TV meteors
Molau (2006)	81	304	−34	40.5									Based on 17 TV meteors
Molau (2006)	82	302.7	−28.5	34.2									Based on 14 TV meteors
Wavelet survey (CMOR)	80.5	304.7	−32.8	38.6	0.02	0.3	1.12	0.9	0.064	56.0	158.6	260.4	
Individual orbits (CMOR)	80.5	305.2	−32.9	38.4			1.09	0.9	0.065	57.0	158.7	260.5	Based on 65 radar orbits

The final two rows show the fits using the wavelet peak positions and linear regression fit to all measured orbits from this work, respectively.

this stream, albeit near the end of the activity period noted by CMOR. This is one of a number of Torodial streams which may owe their existence to very long dynamical residence times and/or long collisional lifetimes (cf. Wiegert, 2007).

Piscis Austrinids (PAU). This shower has been the source of much confusion in the literature, in no small part due to its close proximity in radiant location and time of maximum with the SDA. It is very weak in our data, particularly so in the wavelet data, due to the proximity of the SDA radiant. We find radiant locations 3°–4° north in δ and ∼5° larger in α as compared to the values given in Kashcheyev and Lebedinets (1967) and Ellyett and Roth (1955).

Northern and Southern Iota Aquariids (NIA/SIA). These weak streams suffer significant confusion in the literature due to proximity with the NDA and SDA radiants (cf. Kronk, 1988). The complex of four radiants all lie within the antihelion sporadic source in a circular region less than 10° in radius and all are active over similar time periods in July–August. They are clearly separable in CMOR data as distinct radiants.

It is intriguing to note that the end of the SIA activity near $\lambda = 150°$ is near the start of the STA activity visible first at $\lambda = 165°$. Projection of the linear radiant drift either of the SIA forward or the STA backward from our measured values produces close overlaps with the other stream radiant. Using the longer activity period of the STA and its fit projected backwards produces convincing overlap. Fig. 14 shows the single station radiant location and linear fits for the SIA/STA. Drift in the value of V_g with solar longitude for the STA when projected to the time of the SIA maximum are within 1 km/s of the observed SIA value. This is very suggestive of a link between the two showers—the 15 day interval with no apparent activity is an artifact of our strict selection criteria. Visual examination of the single station radiant activity does show a very weak shower persisting from the end of the SIA activity interval to the beginning of the STA's and connecting the two showers. A similar correspondence exists between the NIA/NTA radiants. That this has not been noted previously may be due to the poor measurement of the radiant drift for the SIA/NIA complex in earlier literature (cf. Rendtel et al., 1995). The literature commonly refers to another strong shower in September (the South & North Delta Piscids, SPI/NPI) as being active (cf. Kronk, 1988), but this is in fact just the start of STA and end of the NIA respectively. We suggest that earlier surveys did not have sufficient continuous temporal coverage to distinguish the NTA/STA and NPI/SPI, though a link was tentatively suggested by Jenniskens (2006). We confirm the linkage, noting that the NPI/SPI do not exist as distinct showers but are part of the NIA/SIA and NTA/STA complex which itself is likely one long-lived continuous shower. If this is correct, the Taurids begin in late July and continue until late November as a single shower, having precessional associations (as noted earlier) with at least the APS and SMA also linked to the NIA/SIA and (by extension) to the NTA and STA.

Perseids (PER). The average velocity measured for the Perseids by CMOR is in error, being ∼2 km/s above the parabolic limit. Some of this error is likely due to overcorrection for atmospheric deceleration; however the uncorrected time of flight

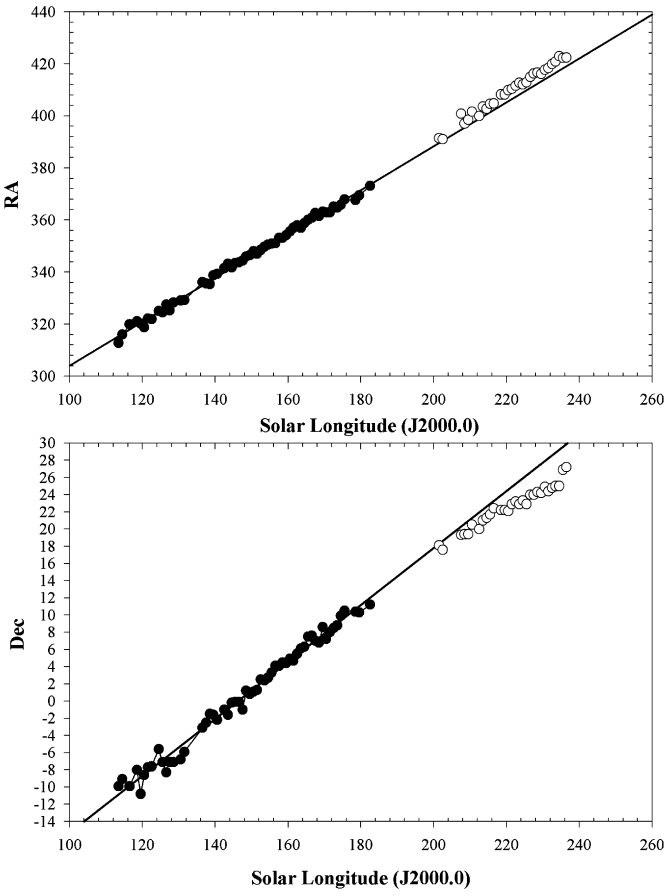

Fig. 14. Radiant drift for the SIA (solid circles) and STA (open circles) from single station data. The linear regression fit from the SIA drift is projected forward for comparison to the location of the STA radiant.

velocity for the Perseids is also slightly hyperbolic. The average velocity found using the hybrid-Fresnel oscillation technique are below the hyperbolic limit suggesting an offset in TOF velocities. Through simulations we have found that the main source of error is due to the radiant geometry relative to one of our outlying stations. The azimuth of the circumpolar Perseid radiant is aligned with the azimuth connecting the Gerber outlying site to the main radar station over a major portion of the maximum visibility of the stream given our radar response function. We find from simulations that this produces a consistent overestimate of ∼1 km/s in the measured velocity.

Daytime Kappa Leonids (KLE). This shower is related via apsidal precession to the November Orionids (NOO)—a connection first suggested by Nilsson (1964)—and both (as well as the December Monocerotids) are likely part of a complex related to Comet D1917 F1 (Mellish). Jenniskens (2006) suggests this stream is the twin of the December Monocerotids, but this association is not clear using the elements for both streams as measured by CMOR.

October Draconids (DRA). This shower appears in our survey solely by virtue of the strength of the outburst in 2005 (cf. Campbell-Brown et al., 2006). Activity in all other years is very close to the background with no more than 1–2 Draconid orbits being recorded in any given "average" year. The geocentric radiant and orbit for the 2005 Draconids given in Campbell-

Brown et al. (2006) is in error due to a computational mistake in the application of the zenith correction term; the values given in this paper should be used instead.

November Orionids (NOO). This is one of the strongest showers in the CMOR catalogue in the latter 1/3rd of the year and is paired with the KLEs. It has been previously called the Xi Orionids by Lindblad and Olsson-Steel (1990) who noted extensive confusion in the literature between the Monocerotids (MON) of December and the Xi Orionids (NOO). Kronk (1988), after examining all the available literature to the mid-1980's, concluded that no strong evidence for two streams exists, but rather suggested the MON constitute one diffuse stream. We conclude here that this is incorrect and note that a clear separation of two streams is visible in CMOR data. The NOO are most prominent in radar surveys and we confirm here the large difference in apparent activity between the NOO and apparently much weaker (at CMOR masses) MON stream. The small difference in velocity (2 km/s) and radiant position ($<10°$ during most of their activity period) of the MON and NOO understandably have led to past mixups between the two streams.

Ursids (URS). As with the Perseids, the unusual radiant geometry relative to the line connecting the main radar site and outlying stations has led to a systematically overestimated velocity for the URS. This is further reflected in the difference between the raw (uncorrected for deceleration) time of flight velocity and the hybrid-Fresnel velocity measurements which show a 1.5 km/s difference. The difference in velocity is just sufficient to move the mean stream orbit from bound to unbound.

Sigma Serpentids (SSE). This new stream shows an extended radiant area, with a maximum in probe size near 5°, among the largest in our survey. The lack of earlier detections is undoubtedly a result of the time of maximum falling in late December, when few of the early surveys were recording. The orbit suggests a probable link with either JFC or HTCs, having undergone significant orbital evolution since ejection.

January Leonids (JLE). This newly recognized shower peaks at nearly the same time as the Quadrantids and is remarkably strong; it is the strongest shower occurring between the maximum times of the Quadrantids and Eta Aquariids based on our single station data. Molau (2006) has also detected this stream in single-station video data (his stream 86) with a radiant within 2° of our position and a velocity only ∼1 km/s higher. The orbit is characteristic of a sungrazing comet. The short duration of the shower and its very tight radiant (wavelet probe size maximum occurs at 1.4° indicating a Gaussian spread of $<1°$) consistent with a very young shower. We suggest this stream may represent the decay products of a sungrazer which has perhaps only recently begun to produce activity at the Earth. The apparent mass distribution in the stream is strongly peaked between +6 and +7; it would be interesting to determine if larger particles are also present in the stream or if it is exclusively rich in small meteoroids. More observations are clearly needed of this new shower.

Alpha Hydrids (AHY). This new shower also shows a preponderance of fainter meteors. It also appears to have been detected by Molau (2006) (his shower 89) though the radiant is more than 5° from our location and the velocity ∼5 km/s lower. As with JLE, this appears to be a stream associated with a long period comet (though not a sungrazer).

Bootid–Coronae Borealid Complex. This complex of three diffuse streams [Theta Coronae Borealids (TCB), Lambda Bootids (LBO); xi Coronae Borealids (XCB)] is unusual in several respects. It shows up obviously in single station data as a broad, diffuse source lasting from $\lambda = 294°$–$303°$, with the three separate radiants detectable in the wavelet analysis of individual radiants. The TCB are the only shower in our list to show a peak probe size at $>8°$; the actual peak is near 14° attesting to the broad nature of the radiant complex and blending between the three stream centers. The TCB are the strongest of these three radiants based on wavelet analysis alone. Sekanina (1976) lists at least three radiants which appear to be linked with this complex (Theta Coronae Borealids, Corona Borealids, and Lambda Bootids). All three radiants have inclinations near 79° and the TCB have a ∼1 and $e < 0.2$ with $q > 0.9$. The high inclination alone rules out the complex as simply an artifact of high collisional probability with the Earth. The broad nature of the streams also suggests that these showers represent a substantial component of the total strength of the North Torodial sporadic source during the month of January. Molau (2006) records activity from this complex between $\lambda = 295°$–$298°$. It is likely that this complex results from the interplay between Poynting–Robertson drag and the Kozai resonance as proposed by Wiegert (2007) starting from an initial JFC-type parent orbit; the large radiant area may indicate significant scattering, possibly from the Earth over long timescales. Kronk (1988) lists a stream he calls the January Bootids as active from a radiant within the Bootid–Coronae Borealid complex, but the velocity he derives is much lower than we measure for any of three component streams in the current survey.

7. Conclusions

From our radar survey we have found 45 showers which meet our selection criteria as real streams. Of this number, 12 are previously unrecognized or poorly characterized. We specifically conclude that:

1. At CMOR masses ($\sim 10^{-7}$ kg) a minimum of 3.4% of all detected meteoroids permitting orbit measurement are found in streams established by our survey. A realistic estimate of the true total number of meteoroids in streams at these masses based on our data is $<10\%$. This emphasizes that the majority of all meteoroids at these masses are sporadic.
2. A high proportion of our detected streams have very low q. This may reflect in part a detection bias; low q meteoroids may be thermally sintered and better able to ablate to lower altitudes (thus avoiding initial radius attenuation). Additionally, low q streams are subject to fast orbital evolution driven by radiation forces (as discussed by Wiegert, 2007), potentially increasing the chances that a trail originally not

intersecting the Earth evolves rapidly to Earth-intersection. It is probable that many of these streams are linked to various sungrazing comet groups (cf. Sekanina and Chodas, 2005); precise linkages require more detailed investigation of orbital evolution, but the measured stream orbital elements presented in this work should enable such studies.

3. The NIA/SIA and NTA/STA (and NPI/SPI showers in the literature) are all linked and represent the same stream. CMOR data shows a nearly continuous coherent contribution from the Taurid stream between July and November each year. This further supports the contention of Whipple (1967) and Porubcan and Stohl (1987) regarding the dominance of the Taurid complex in connection with the sporadic background as a whole. We emphasize that these streams are located in the antihelion source but show radiant sizes much smaller than the AH source (cf. Campbell-Brown, 2007).
4. Several streams show a substantial deficit of larger meteoroids, notably the NOO and SZC. These "radar" streams are weak or non-existent in much of the literature due to use of datasets often dominated by larger meteoroids. Our magnitude distribution for these streams also shows a pronounced skewness to smaller masses, quite distinct from other streams. This would seem to indicate much steeper than normal mass distribution indices, though this needs confirmation through direct measurement, a topic of a future work.

As additional orbits are added to the CMOR dataset we expect to detect weaker showers, some of which are clearly visible in manual examination of the dataset (but just barely fail to make our current selection criteria).

Acknowledgments

P.B. thanks the Canada Research Chair program, the Natural Sciences and Engineering Research Council and the NASA Meteoroid Environment Office for funding support. The authors gratefully acknowledge the invaluable technical assistance of K. Ellis and Z. Krzeminski in day to day radar operations. The orbital routines used in CMOR analysis were kindly provided by Z. Ceplecha. V. Porubcan and J. Drummond provided helpful comments on an earlier version of this manuscript.

References

Antoine, J.P., 2004. Two Dimensional Wavelets and Their Relatives. Cambridge Univ. Press, Cambridge, UK, 476 pp.

Andrianov, N.S., Kurganov, R.A., Nasirov, A.M., Sidorov, V.V., 1968. Oblique scattering method for measuring individual radiants and meteor velocities. In: Kresak, L., Millman, P.M. (Eds.), IAU Symposium 33: Physics and Dynamics of Meteors, pp. 14–26.

Andrianov, N.S., Pupyusev, U.A., Sidorov, V.V., 1970. The distribution of orbit parameters and changes in incident meteor particle flux density. Mon. Not. R. Astron. Soc. 148, 227–237.

Babadzhanov, P.B., Kramer, E.N., 1967. Orbits of bright photographic meteors. Smithson. Contrib. Astrophys. 11, 67–79.

Baggaley, W.J., 1995. Radar surveys of meteoroid orbits. Earth Moon Planets 68, 127–139.

Baggaley, W.J., Bennett, R.G.T., Steel, D.I., Taylor, A.D., 1994. The Advanced Meteor Orbit Radar Facility—AMOR. Quart. J. R. Astron. Soc. 35, 293.

Bailey, M.E., Chambers, J.E., Hahn, G., 1992. Origin of sungrazers—A frequent cometary end-state. Astron. Astrophys. 257, 315–322.

Bendjoya, P., Slezak, E., Froeschle, C., 1991. The wavelet transform—A new tool for asteroid family determination. Astron. Astrophys. 251, 312–330.

Betlem, H., et al., 1995. DMS Photographic Meteor Database. Leiden.

Betlem, H., Kuile, C.T., van't Leven, J., de Lignie, M., Bellot Rubio, L.R., Koop, M., Angelo, C., Wilson, M., Jenniskens, P., 1997. Precisely reduced meteoroid trajectories and orbits from the 1995 Leonid meteor outburst. Planet. Space Sci. 45, 853–856.

Borovicka, J., Koten, P., Spurny, P., Bocek, J., Stork, R., 2005. A survey of meteor spectra and orbits: Evidence for three populations of Na-free meteoroids. Icarus 174, 15–30.

Brown, P., Jones, J., Weryk, R.J., Campbell-Brown, M.D., 2004. The velocity distribution of meteoroids at the Earth as measured by the Canadian Meteor Orbit Radar (CMOR). Earth Moon Planets 95, 617–626.

Burke, J.G., 1986. Cosmic Debris: Meteorites in History. Univ. of California Press, Los Angeles, 445 pp.

Campbell-Brown, M.D., 2004. Arietid meteor orbits measurements. Earth Moon Planets 95, 297–301.

Campbell-Brown, M., 2007. The meteoroid environment: Shower and sporadic meteors. In: Krueger, H., Graps, A. (Eds.), Dust in Planetary Systems, ESA SP-643. European Space Agency, Noordwijk, pp. 11–21.

Campbell-Brown, M.D., Hildebrand, A., 2004. A new analysis of fireball data from the Meteorite Observation and Recovery Project (MORP). Earth Moon Planets 95, 489–499.

Campbell-Brown, M., Vaubaillon, J., Brown, P., Weryk, R.J., Arlt, R., 2006. The 2005 Draconid outburst. Astron. Astrophys. 451, 339–344.

Ceplecha, Z., 1957. Photographic Geminids 1955. Bull. Astron. Inst. Czech. 8, 51–61.

Ceplecha, Z., Jevzkova, M., Novak, M., Rajchl, J., Sehnal, L., Davies, J.G., 1964. Ondrejov double-station meteors during the IGY and IGC. Bull. Astron. Inst. Czech. 15, 144–155.

Cook, A.F., 1973. A working list of meteor streams. In: IAU Colloq. 13: Evolutionary and Physical Properties of Meteoroids, p. 183.

Davies, J.G., Gill, J.C., 1960. Radio echo measurements of the orbits of faint sporadic meteors. Mon. Not. R. Astron. Soc. 121, 437–462.

Denning, W.F., 1899. General catalogue of the radiant points of meteoric showers and of fireballs and shooting stars observed at more than one station. Mem. R. Astron. Soc. 53, 203–292.

Drummond, J.D., 1981. A test of comet and meteor shower associations. Icarus 45, 545–553.

Ellyett, C.D., Roth, K.W., 1955. The radar determination of meteor showers in the southern hemispheres. Aust. J. Phys. 8, 390–401.

Fedynski, V.V., 1975. Meteor Orbits and Rates from Equatorial Survey, vol. 1. Materials of the World Data Center B. Soviet Geophysical Committee of the Academy of Sciences of the USSR, Moscow.

Fedynski, V.V., 1977. Meteor Orbits and Rates from Equatorial Survey, vol. 2. Materials of the World Data Center B. Soviet Geophysical Committee of the Academy of Sciences of the USSR, Moscow.

Gartrell, G., Elford, W.G., 1975. Southern hemisphere meteor stream determinations. Aust. J. Phys. 28, 591–620.

Galligan, D.P., 2000. Structural analysis of radar meteoroid orbital data, Doctoral Dissertation, University of Canterbury, 427 pp.

Galligan, D.P., Baggaley, W.J., 2002a. Wavelet enhancement for detecting shower structure in radar meteoroid data. II. Application to the AMOR data. In: Green, S.F., Williams, I.P., McDonnell, J.A.M., McBride, N. (Eds.), IAU Colloq. 181: Dust in the Solar System and Other Planetary Systems. Pergamon Press, Amsterdam, p. 48.

Galligan, D.P., Baggaley, W.J., 2002b. Wavelet enhancement for detecting shower structure in radar meteoroid data. I. Methodology. In: Green, S.F., Williams, I.P., McDonnell, J.A.M., McBride, N. (Eds.), IAU Colloq.181: Dust in the Solar System and Other Planetary Systems. Pergamon Press, Amsterdam, p. 42.

Galligan, D.P., Baggaley, W.J., 2005. The radiant distribution of AMOR radar meteors. Mon. Not. R. Astron. Soc. 359, 551–560.

Halliday, I., 1988. Geminid fireballs and the peculiar Asteroid 3200 Phaethon. Icarus 76, 279–294.
Halliday, I., Griffin, A.A., Blackwell, A.T., 1996. Detailed data for 259 fireballs from the Canadian camera network and inferences concerning the influx of large meteoroids. Meteorit. Planet. Sci. 31, 185–217.
Hawkins, G.S., Southworth, R.B., 1961. Orbital elements of meteors. Smithsonian Contrib. Astrophys. 4, 85–96.
Hocking, W.K., 2000. Real-time meteor entrance speed determinations made with interferometric meteor radars. Radio Sci. 35, 1205–1220.
Hocking, W.K., Fuller, B., Vandepeer, B., 2001. Real-time determination of meteor-related parameters utilizing modern digital technology. J. Atmos. Solar–Terr. Phys. 63, 155–169.
Hoffmeister, C., 1948. Meteorstrome: Meteoric Currents. J.A. Barth, Leipzig.
Hughes, D.W., 1990. The mass distribution of comets and meteoroid streams and the shower/sporadic ratio in the incident visual meteoroid flux. Mon. Not. R. Astron. Soc. 245, 198–203.
Jacchia, L.G., Whipple, F.L., 1961. Precision orbits of 413 photographic meteors. Smithsonian Contrib. Astrophys. 4, 97–129.
Jenniskens, P., 1994. Meteor stream activity. I. The annual streams. Astron. Astrophys. 287, 990–1013.
Jenniskens, P., 2004. 2003 EH1 is the Quadrantid shower parent comet. Astron. J. 127, 3018–3022.
Jenniskens, P., 2006. Meteor Showers and Their Parent Comets. Cambridge Univ. Press, Cambridge, UK, 790 pp.
Jones, J., Brown, P., 1993. Sporadic meteor radiant distributions—Orbital survey results. Mon. Not. R. Astron. Soc. 265, 524.
Jones, J., Jones, W., 2006. Meteor radiant activity mapping using single-station radar observations. Mon. Not. R. Astron. Soc. 367, 1050–1056.
Jones, J., Webster, A.R., Hocking, W.K., 1998. An improved interferometer design for use with meteor radars. Radio Sci. 33, 55–65.
Jones, J., Brown, P., Ellis, K.J., Webster, A.R., Campbell-Brown, M.D., Krzemenski, Z., Weryk, R.J., 2005. The Canadian Meteor Orbit Radar (CMOR): System overview and preliminary results. Planet. Space Sci. 53, 413–421.
Jopek, T.J., 1993. Remarks on the meteor orbital similarity D-criterion. Icarus 106, 603–607.
Jopek, T.J., Froeschle, C., 1997. A stream search among 502 TV meteor orbits: An objective approach. Astron. Astrophys. 320, 631–641.
Jopek, T.J., Valsecchi, G.B., Froeschle, C., 1999. Meteoroid stream identification: A new approach. II. Application to 865 photographic meteor orbits. Mon. Not. R. Astron. Soc. 304, 751–758.
Kashcheyev, B.L., Lebedinets, V.N., 1967. Radar studies of meteors. In: Hawkins, G.S. (Ed.), Meteor Orbits and Dust. NASA, Washington, DC, p. 183.
Kashcheev, B.L., Tkachuk, A.A., 1980. Rezul'taty radiolokatsionnykh nabliudenii slabykh meteorov: Katalog orbit meteorov do +12 m. Moskva [s.n.], 1980.
Katasev, L.A., 1964. Photographic Methods in Meteor Astronomy. IPST, Jerusalem.
Koten, P., Borovicka, J., Spurny, P., Betlem, H., Evans, S., 2004. Atmospheric trajectories and light curves of shower meteors. Astron. Astrophys. 428, 683–690.
Kresak, L., Porubcan, V., 1970. The dispersion of meteors in meteor streams. I. The size of the radiant areas. Bull. Astron. Inst. Czech. 21, 153–170.
Kronk, G.W., 1988. Meteor Showers: A Descriptive Catalogue. Enslow Publishers, Hillside, NJ.
Lebedinets, V.N., 1968. Radar Meteor Orbits. In: Kresak, L., Millman, P.M. (Eds.), IAU Symposium 33: Physics and Dynamics of Meteors, pp. 241–264.
Lebedinets, V.N., Korpusov, V.N., Manokhina, A.V., 1981. Radiolokatsionnye Issledovaniia Meteorov V Obninske: Katalog Orbit, Sentiabr'–Dekabr' 1967. Mezhduvedomstvennyi Geofizicheskii Kom-t pri Prezidiume AN SSSR, Moskva.
Lebedinets, V.N., Korpusov, V.N., Manokhina, A.V., 1982. Radiolokatsionnye Issledovaniia Meteorov V Obninske: Katalog Orbit, Ianvar'–Avgust 1968. Mezhduvedomstvennyi Geofizicheskii Kom-t pri Prezidiume AN SSSR, Moskva.
Lindblad, B.A., 1971. A computerized stream search among 2401 photographic meteor orbits. Smithsonian Astrophys. Observ. Contrib. Astrophys. 12, 14–24.
Lindblad, B.A., 1987. The IAU meteor data center in Lund. Astron. Inst. Czechoslovak Acad. Sci. 67, 201–204.
Lindblad, B.A., 1991. The IAU Meteor Data Center in Lund. In: Levasseur-Regourd, A.C., Hasegawa, H. (Eds.), IAU Colloq. 126: Origin and Evolution of Interplanetary Dust, vol. 173. Kluwer Academic Publishers, Dordrecht, p. 311.
Lindblad, B.A., Olsson-Steel, D., 1990. The Monocerotid meteor stream and Comet Mellish. Bull. Astron. Inst. Czech. 41, 193–200.
Lindblad, B.A., Neslusan, L., Porubcan, V., Svoren, J., 2003. IAU meteor database of photographic orbits version 2003. Earth Moon Planets 93, 249–260.
Lovell, A.C.B., 1954. Meteor Astronomy. Clarendon, Oxford.
McIntosh, R.A., 1935. An index to southern meteor showers. Mon. Not. R. Astron. Soc. 95, 709–718.
McCrosky, R.E., Posen, A., 1961. Orbital elements of photographic meteors. Smithsonian Contrib. Astrophys. 4, 15–84.
McCrosky, R.E., Shao, C.Y., Posen, A., 1978. Prairie network fireballs. I. General information and orbits. Meteoritika 37, 44–59.
Molau, S., 2006. How good is the IMO Working list of meteor showers? A complete analysis of the IMO video meteor database. In: Proc. Int. Meteor Conf. 2006. International Meteor Organization, Potsdam.
Nilsson, C.S., 1964. A southern hemisphere radio survey of meteor streams. Aust. J. Phys. 17, 205.
Oberst, J., Molau, S., Heinlein, D., Gritzner, C., Schindler, M., Spurny, P., Ceplecha, Z., Rendtel, J., Betlem, H., 1998. The European Fireball Network: Current status and future prospects. Meteorit. Planet. Sci. 33, 49–56.
Ohtsuka, K., Nakano, S., Yoshikawa, M., 2003. On the association among periodic Comet 96P/Machholz, Arietids, the Marsden comet group, and the Kracht comet group. Publ. Astron. Soc. Jpn. 55, 321–324.
Porubcan, V., Stohl, J., 1987. The meteor complex of P/Encke. In: European Regional Astronomy Meeting of the IAU, vol. 22, pp. 167–171.
Reach, W.T., Kelley, M.S., Sykes, M.V., 2007. A survey of debris trails from short-period comets. ArXiv e-print arXiv:0704.2253.
Rendtel, J., Arlt, R., McBeath, A., 1995. Handbook for Visual Meteor Observers, International Meteor Organization Monograph No. 2. International Meteor Organisation, Potsdam. 308 pp.
Sarma, T., Jones, J., 1985. Double-station observations of 454 TV meteors. I. Trajectories. Bull. Astron. Inst. Czech. 36, 9–24.
Sekanina, Z., 1976. Statistical model of meteor streams. IV. A study of radio streams from the synoptic year. Icarus 27, 265–321.
Sekanina, Z., 1973. Statistical model of meteor streams. III. Stream search among 19303 radio meteors. Icarus 18, 253–284.
Sekanina, Z., Chodas, P.W., 2005. Origin of the Marsden and Kracht groups of sunskirting comets. I. Association with Comet 96P/Machholz and its interplanetary complex. Astrophys. J. Suppl. Ser. 161, 551–586.
Southworth, R.B., Hawkins, G.S., 1963. Statistics of meteor streams. Smithsonian Contrib. Astrophys. 7, 261–286.
Sykes, M.V., Walker, R.G., 1992. Cometary dust trails. I. Survey. Icarus 95, 180–210.
Tiscareno, M.S., Burns, J.A., Nicholson, P.D., Hedman, M.M., Porco, C.C., 2007. Cassini imaging of Saturn's rings. Icarus 189, 14–34.
Tedesco, E.F., Harvey, G.A., 1976. Trajectories and orbits from the NASA-NMSU meteor observatory. I. Astron. J. 81, 1010–1013.
Ueda, M., Fujiwara, Y., Sugimoto, M., Kinoshita, M., 2001. Results of double-station TV observations in 1998 and 1999. In: Meteoroids 2001 Conference 495, pp. 325–330.
Vaubaillon, J., Jenniskens, P., 2007. Dust trail evolution applied to long-period Comet C/1854 L1 (Klinkerfues) and the epsilon-Eridanids. Adv. Space Res. 39, 612–615.
Valsecchi, G.B., Jopek, T.J., Froeschle, C., 1999. Meteoroid stream identification: A new approach. I. Theory. Mon. Not. R. Astron. Soc. 304, 743–750.
Verniani, F., 1973. An analysis of the physical parameters of 5759 faint radio meteors. J. Geophys. Res. 78, 8429–8462.
Webster, A.R., Brown, P.G., Jones, J., Ellis, K.J., Campbell-Brown, M., 2004. Canadian Meteor Orbit Radar (CMOR). Atmos. Chem. Phys. Discuss. 4, 1181–1201.
Weiss, A., 1960. Radio-echo observations of southern hemisphere meteor shower activity from 1956 December to 1958 August. Mon. Not. R. Acad. Sci. 120, 387–403.

Wiegert, P.A., 2007. The dynamics of low-perihelion meteoroid streams. Earth Moon Planets, doi:10.1007/s11038-007-9182-2, in press.
Whipple, F.L., 1951. The Baker super-Schmidt meteor cameras. Astron. J. 56, 144–145.
Whipple, F.L., 1954. Photographic meteor orbits and their distribution in space. Astron. J. 59, 201–217.
Whipple, F.L., 1967. On maintaining the meteoritic complex. In: The Zodiacal Light and Interplanetary Medium. NASA-SP150, pp. 409–426.
Whipple, F.L., 1983. 1983 TB and the Geminid meteors. IAU Circ. 3881.
Wright, F., Jacchia, L.G., Whipple, F., 1956. Photographic alpha-Capricornid meteors. Astron. J. 61, 61.
Wiegert, P., Brown, P., 2004. The problem of linking minor meteor showers to their parent bodies: Initial considerations. Earth Moon Planets 95, 19–26.
Yrjola, I., Jenniskens, P., 1998. Meteor stream activity. VI. A survey of annual meteor activity by means of forward meteor scattering. Astron. Astrophys. 330, 739–752.